LU-TP 21-16
June 2021

Radiative Corrections Beyond the Soft-Photon Approximation

Jacob Lindahl

Department of Astronomy and Theoretical Physics, Lund University

Bachelor thesis supervised by Johan Bijnens and Tomáš Husek

LUND
UNIVERSITY

Abstract

This thesis calculates the bremsstrahlung correction beyond the soft-photon approximation for the decay $\omega \to \pi^0 l^+ l^-$. The effect of the radiative corrections on the extraction of the transition form factor from data is investigated. Four different form-factor models are used to compute corrections: vector-meson dominance, lowest-meson dominance, tree-level, and two-hadron saturation. The experimental data used for applying the corrections were taken from the NA60, A2, and Lepton-G experiments. The result of these corrections and their implications are evaluated and discussed.

Popular Science Description

Approximations are the lifeblood of physicists. Without them, problems in everything from Classical Mechanics to Quantum Mechanics can become impossible (or at least extremely tedious) to solve. When models are constructed, choosing right approximations in what phenomena can be ignored or not can be crucial in order to describe and imitate reality. Determining whether or not too many approximations were made (i.e. too many phenomena were ignored) or if there are new physical phenomena at work when a model no longer corresponds with reality is an essential part of physics research. This is especially vital within particle physics where the number of interactions necessitates numerous approximations. Evaluating these approximations can then provide an insight into the effectiveness of these models in describing reality.

An area of physics where this becomes apparent is in form-factor modelling. Form factors are like mystery boxes that seek to capture the full complexity of an interaction that cannot be calculated by hand. Due to their opaque nature they are determined from experimental data. This has of course not stopped physicists from developing a series of different models to try and predict the behavior of these form factors. However, when comparing these theoretical models to experiments there is sometimes a deviation for certain particle decays that cannot be explained by uncertainty in the data. This forces us to confront whether or not these models are inherently flawed or if they can be remedied.

This type of deviation is seen in the Dalitz decays of the ω vector meson. When the transition form factor has been measured and then compared with theoretical models for the form factor a deviation is clearly seen. When these form factor models were constructed, only some phenomena were included under the assumption that this would capture enough of the interaction. One way to determine the effectiveness of these models is then to determine if including more complex aspects of the interaction could eliminate this deviation.When it comes to quantum electrodynamics (QED) approximations are also made to determine the decay widths (or probability) of decays. Going beyond the simplest (or leading order) approximation can then include computing the radiative corrections one of which is the bremsstrahlung contribution. The bremsstrahlung phenomenon involves having one (or more) of the particles involved in the decay emit a photon.

This often makes the calculation for the decay width far more complicated unless, again, some approximation is introduced. One possible way to simplify the calculation is the soft-photon approximation where the energy of the photon is assumed to be small (or soft). When this calculation is attempted, a singularity (infinity) appears when the photon energy becomes small. These infinite quantities are then cancelled when other radiative corrections are included. However, this ignores the full range of possible energy values for the photon. This means when the form factor is measured, the estimate is affected by radiative corrections stemming from ignoring these energetic photons. Ignoring these corrections could then be the reason for the deviation between theory and experiment.

The goal of this thesis is to explore if computing the radiative corrections and going beyond the soft-photon approximation can eliminate the deviation seen between the different form factor models and the experimental data for the ω vector meson decays under consideration. If this deviation fails to disappear then new approaches consistent with (or not consistent with) the Standard Model are needed. Regardless of the overall effectiveness of the radiative corrections in this particular case, they should still be used when comparing form factor models and experiment.

Contents

Acknowledgments

I would like to give special thanks to my supervisors Johan Bijnens and Tomáš Husek for their invaluable help and comments during this work. I would also like to thank my family for fruitful discussions and support.

List of acronyms

BS Bremsstrahlung

CMS Center-of-mass system

EM Electromagnetic

FF Form factor

IR Infrared

LMD Lowest-meson dominance

LO Leading-order

NLO Next-to-leading order

QCD Quantum Chromodynamics

QED Quantum Electrodynamics

QFT Quantum field theory

VMD Vector-meson dominance

SM Standard Model

TL Tree-level

THS Two-hadron saturation

Notes on Notation

- Throughout the thesis natural units ($\hbar = c = 1$) are used.
- The four-momentum of a particle or object is denoted by p while the spatial momentum is denoted by $\mathbf{p}$.
- The notation $\not{p}$ is used for the contraction of gamma matrices and four-momentum vectors such that $\not{p} = \gamma^\mu p_\mu$.
- The notation $p_{1,i}$ refers to the ith element of the p_1 four-vector.

1 Introduction

In the framework of modern physics, approximations are essential to gain numerical results. Without them, many calculations would become intractable or simply too unwieldy to be useful. Most approximations are motivated by theory or necessity such as the simple case of ignoring friction in classical mechanics. This need for approximations becomes more and more apparent within the realm of particle physics where calculations can quickly become immensely complex without appropriate approximations [1].

This need is especially apparent in quantum field theory (QFT). In Quantum Chromodynamics (QCD), attempts to calculate the interaction between hadrons quickly escalates in complexity making it essentially impossible to get analytical solutions. Trying to account for all involved quarks and gluons as well as virtual quark-antiquark pairs then often boils down to studying phenomenological quantities that can give insight into these complex interactions [1, 2]. As a result, to properly describe the internal structure of hadrons, form factors (FF) are introduced. These can be experimentally determined or can be modeled theoretically. Examples of this are electromagnetic (EM) transition form factors that reflect the internal charge and current distributions inside the hadrons. Thereby the entire internal structure of the hadrons can be probed using these quantities [1, 2].

These form factors are quantities with the structure only being probed using experimental data. Using principles from QED and QCD, this has of course led to the development of numerous models to try and predict the behavior of the form factors over a range of exchanged momentum values for the interaction [2]. When designing these models, physicists make decisions on what assumptions to make and what contributions to take into account. With many of these models, a deviation can be seen when comparing the theoretical and experimental results for certain decays. One possible explanation for this deviation comes from failing to account for the full range of radiative corrections stemming from QED. This is from either ignoring them entirely or through the invoking of the soft-photon approximation in the bremsstrahlung (BS) contribution. In this approximation the energy of the emitted BS photon is assumed to be small (or soft). This simplifies the calculations but ignores the possible contribution from the BS photons with energy above a certain threshold. The computation of the radiative corrections piece by piece also introduces infrared (IR) divergences that are cancelled by considering the total radiative corrections.

Going beyond the soft-photon approximation would help to properly disentangle the electromagnetic and hadronic effects from each other, and possibly resolve the deviation seen between experimental data and the form factor models. Looking at a process such as the Dalitz decay $\omega \to \pi^0 \ell^+ \ell^-$ (with ℓ standing for electrons or muons) provides a good opportunity to attempt to compute these radiative corrections, apply them to experimental data and determine whether or not other physical phenomena need to be included to these form factor models and if one can make theory and experiment align more closely.

This thesis is structured with Section 2 introducing the background behind the decay $\omega \to \pi^0 \ell^+ \ell^-$ and the necessary information about radiative corrections. Subsection 2.4 outlines the bremsstrahlung phenomenon and correction. The solution for going beyond the soft-photon approximation is also presented. In Section 3 the procedure for implementing and computing the corrections is outlined. Section 4 introduces the results from the computations and shows the result of applying the corrections. Finally, in Section 5 the result of these corrections are discussed. The effectiveness in removing the deviation is discussed, as well as avenues of research opened by the result.

2 Theoretical Background

2.1 The Decay $\omega \to \pi^0 \ell^+ \ell^-$

The ω meson is a neutral vector meson that has quark content consisting of a nearly pure symmetric $u\bar{u}$ and $d\bar{d}$ state that can be written as $(u\bar{u} + d\bar{d})/\sqrt{2}$. Its main decay modes include the decay $\omega \to \pi^0\pi^+\pi^-$ and the decay $\omega \to \pi^0\gamma$ where the π^0 meson is a neutral pseudoscalar meson [3]. Decays of the type $A \to B + \gamma$, where A and B are mesons and γ is a photon, are called electromagnetic radiative decays. In these types of decays, the emitted photon can undergo internal conversion and turn into a lepton pair. These types of decays are then called conversion decays [4]. The ω meson can, in fact, also decay through this type of decay in the form $\omega \to \pi^0 \ell^+ \ell^-$ where ℓ can either be a muon or electron [3]. To describe the decay, QED is used for the electromagnetic nature of the decay as the ω meson decays to the π^0 meson and the virtual (off-shell) photon further turning into the lepton pair. To model this interaction completely, taking into account all the different interactions, is inherently complicated. As such, to capture the total internal EM structure of the decay, an EM form factor is introduced that then contains all the information about the internal structure of the decay not included in the theoretical approximation [4]. The form factor is a quantity that can be extracted from analyzing the probability of the decay as a function of the invariant mass squared q^2 of the photon in the ω Dalitz decay, corresponding to the invariant mass of the lepton pair [4]. The probability per invariant mass squared is called the invariant mass spectrum and is denoted by $\mathrm{d}\Gamma/\mathrm{d}q^2$, where Γ is the width of the decay. Theoretically, the width of the decay can be determined using QED with internal EM structure of the meson interaction found within the form factor data. The FF can be denoted $\mathcal{F}_\omega(q^2)$ and for the normalized FF at $q^2 = 0$ we use $\hat{\mathcal{F}}_\omega(q^2)$. The invariant mass spectrum $\mathrm{d}\Gamma/\mathrm{d}q^2$ can then be related to the normalized FF via

$$\frac{\mathrm{d}\Gamma}{\mathrm{d}q^2} = \left.\frac{\mathrm{d}\Gamma}{\mathrm{d}q^2}\right|_{\text{Point}} |\hat{\mathcal{F}}_\omega(q^2)|^2 \,, \tag{1}$$

where $\mathrm{d}\Gamma/\mathrm{d}q^2|_{\text{Point}}$ refers to the QED prediction for the overall decay width with ω treated as point-like [4]. The estimate for $|\hat{\mathcal{F}}_\omega(q^2)|^2$ then naturally depends on the theoretical determination of $\mathrm{d}\Gamma/\mathrm{d}q^2|_{\text{Point}}$ using QED and the experimental data for $\mathrm{d}\Gamma/\mathrm{d}q^2$.

2.2 The $\omega \to \pi^0 \ell^+ \ell^-$ Decay at Leading-order

The differential decay width of the $\omega \to \pi^0 \ell^+ \ell^-$ decay needs to be calculated to determine the FF. Similar discussion for the differential decay widths can be seen in Ref. [5] and Ref. [6]. The Feynman diagram of the leading-order (LO) contribution in the QED expansion can be seen in Fig. 1. In the decay, the four-momenta of the ω meson, the π^0 meson, the lepton ℓ^-, and the antilepton ℓ^+ are labelled as p_1, p_2, q_1, and q_2, respectively. Then, from conservation of energy and momentum, we have

$$p_1 = p_2 + q_1 + q_2 \,.$$

The matrix element for this decay can then be extracted from Fig. 1 using Feynman rules. It is found to be [7]

$$i\mathcal{M}^{\text{LO}}_{\omega\to\pi^0 l^+ l^-} = ie\mathcal{F}_\omega(q^2)\epsilon^{\mu\nu\alpha\beta} p_{1\alpha} q_\beta \epsilon_\mu(\mathbf{p}_1) \frac{(-i)}{q^2} \bar{u}(\mathbf{q}_1)(-ie\gamma_\nu)v(\mathbf{q}_2) \,, \tag{2}$$

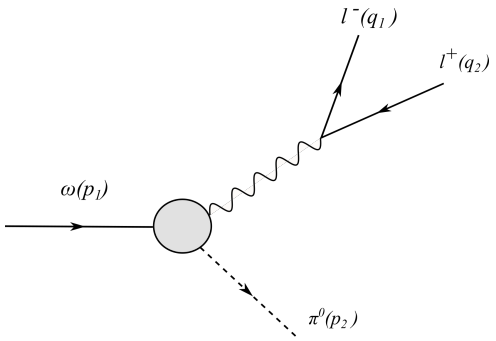

Figure 1: The LO Feynman diagram of the decay $\omega \to \pi^0 \ell^- \ell^+$. The shaded blob corresponds to the FF.

where $\mathcal{F}_\omega(q^2)$ is the form factor represented by the gray blob as seen in Fig. 1, and $q = q_1 + q_2$ is the four-momentum of the lepton pair. Before proceeding with considering the rest of the calculation for the differential decay width, some dimensionless variables can be introduced using the notation from Ref. [6]. We can define a variable x as the normalized square of the total energy of the lepton–antilepton pair in its center-of-mass system (CMS) such that

$$x = \frac{(q_1 + q_2)^2}{\Delta_M^2}\,. \tag{3}$$

Here $\Delta_M = m_\omega - m_\pi$ where m_ω is the rest mass of the ω meson and m_π is the rest mass of the π^0 meson. The rescaled cosine of the angle between the directions of the decaying ω meson and the antilepton in the lepton–antilepton CMS is denoted by y,

$$y = \frac{2p_1 \cdot (q_1 - q_2)}{\lambda^{\frac{1}{2}}(p_1^2, p_2^2, (q_1 + q_2)^2)}\,, \tag{4}$$

where λ is the Källén function of the form

$$\lambda(a, b, c) = a^2 + b^2 + c^2 - 2ab - 2ac - 2bc\,. \tag{5}$$

For convenience we can define $\lambda(x)$ as

$$\lambda(x) \equiv \lambda(m_\omega^2, m_\pi^2, \Delta_M^2 x)\,. \tag{6}$$

Other related convenient definitions employed later are $\Delta_m^2 = 2p_1 \cdot (q_1 - q_2) = y\lambda^{\frac{1}{2}}(x)$ and $s = (q_1 + q_2)^2 = \Delta_M^2 x$. We can also consider the limits imposed on the x and y variables possible values. For convenience, another constant ν can be introduced defined as $\nu = 2m/\Delta_M$ with m being mass of one of the final-state leptons. Now looking at the definition of x in Eq. (3), the minimum possible value would occur when $(q_1+q_2)^2 = 4m^2$. So using the definition for ν one finds that the lowest possible value is ν^2. The maximum value for x is 1 when $(q_1 + q_2)^2 = \Delta_M^2$ such that the limits on x are $x \in [\nu^2, 1]$. For the limits on y, another variable β is convenient, defined as

$$\beta = \beta(x) = \sqrt{1 - \frac{\nu^2}{x}}\,. \tag{7}$$

Here, β is the speed of the leptons in their CMS. Another related variable γ used later can also be introduced and is defined as

$$\gamma = \gamma(x) = \frac{1-\beta(x)}{1+\beta(x)}\,. \tag{8}$$

The limits on y then become $y \in [-\beta, \beta]$ [6]. The LO matrix element squared can now be written as

$$\overline{|\mathcal{M}^{\mathrm{LO}}(x,y)|^2} = \frac{8\pi^2\alpha^2\lambda(x)}{3\Delta_M^2 x}|\mathcal{F}_\omega(x\Delta_M^2)|^2\left(1+\frac{\nu^2}{x}+y^2\right), \tag{9}$$

where α is the fine-structure constant. The two-fold differential decay width can then be written as

$$\frac{\mathrm{d}^2\Gamma(x,y)}{\mathrm{d}x\mathrm{d}y} = \frac{\Delta_M^2\lambda^{\frac{1}{2}}(x)}{512\pi^3 m_\omega^3}\overline{|\mathcal{M}(x,y)|^2}\,, \tag{10}$$

where $\overline{|\mathcal{M}(x,y)|^2}$ is the matrix element squared, of the interaction [7]. Hence using the LO matrix element squared, the total two-fold differential decay width for the decay at LO is

$$\frac{\mathrm{d}^2\Gamma^{\mathrm{LO}}(x,y)}{\mathrm{d}x\mathrm{d}y} = \frac{\alpha^2\lambda^{\frac{3}{2}}(x)}{192\pi m_\omega^3 x}|\mathcal{F}_\omega(\Delta_M^2 x)|^2\left(1+\frac{\nu^2}{x}+y^2\right). \tag{11}$$

It is also convenient to integrate away the dependence on y to get the differential decay width with respect to x only, which becomes

$$\frac{\mathrm{d}\Gamma^{\mathrm{LO}}(x)}{\mathrm{d}x} = \int_{-\beta}^{\beta}\frac{\mathrm{d}^2\Gamma^{\mathrm{LO}}(x,y)}{\mathrm{d}x\mathrm{d}y}\mathrm{d}y = \frac{\alpha^2\beta\lambda^{\frac{3}{2}}(x)}{72\pi m_\omega^3 x}|\mathcal{F}_\omega(\Delta_M^2 x)|^2\left(1+\frac{\nu^2}{2x}\right). \tag{12}$$

The NLO contribution can be written as a correction term δ to the LO differential decay width so that we can write

$$\mathrm{d}\Gamma(x,y) = \mathrm{d}\Gamma^{\mathrm{LO}}(x,y) + \mathrm{d}\Gamma^{\mathrm{NLO}}(x,y) + \ldots = (1+\delta(x,y)+\ldots)\mathrm{d}\Gamma^{\mathrm{LO}}(x,y)\,. \tag{13}$$

Ignoring higher order terms beyond NLO, the NLO correction in terms of x and y, $\delta(x,y)$, can then be defined as

$$\delta(x,y) = \frac{\mathrm{d}^2\Gamma^{\mathrm{NLO}}(x,y)}{\mathrm{d}x\mathrm{d}y}\Bigg/\frac{\mathrm{d}^2\Gamma^{\mathrm{LO}}(x,y)}{\mathrm{d}x\mathrm{d}y}\,, \tag{14}$$

using Eq. (13). The dependence on y can also be removed as in Eq. (12) to give $\delta(x)$. Using that Eq. (14) is a ratio, the term $\mathrm{d}^2\Gamma^{\mathrm{NLO}}(x,y)/\mathrm{d}x\mathrm{d}y$ needs to be integrated over y and combined with Eq. (12) so that we can write

$$\delta(x) = \left[\frac{\mathrm{d}\Gamma^{\mathrm{LO}}(x)}{\mathrm{d}x}\right]^{-1}\int_{-\beta}^{\beta}\delta(x,y)\left[\frac{\mathrm{d}^2\Gamma^{\mathrm{LO}}(x,y)}{\mathrm{d}x\mathrm{d}y}\right]\mathrm{d}y\,. \tag{15}$$

The NLO correction comes from the contributions of several different diagrams and can be split up into different components as

$$\delta = \delta^{\mathrm{BS}} + \delta^{\mathrm{Virtual}}\,. \tag{16}$$

Here δ^{BS} is from the BS contribution and $\delta^{\mathrm{virtual}}$ from the virtual contribution. First we consider the virtual contributions.

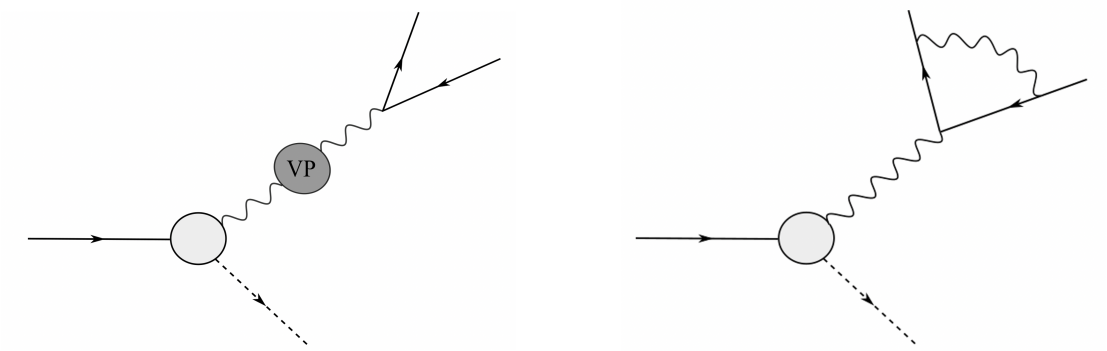

(a) Vacuum Polarization

(b) Vertex Correction

Figure 2: NLO virtual corrections in the QED expansion on the lepton side. (a) shows the vacuum-polarization-insertion contribution to the photon propagator with the shaded region denoting lepton loops and hadronic contributions. (b) shows the QED vertex correction at NLO.

2.3 Virtual Corrections

The virtual corrections arise from the interference term of the LO diagram shown in Fig. 1 and the NLO diagrams shown in Figs. 2a and 2b [8]. Once again, similar discussions can be seen in Ref. [5] and Ref. [6]. We only consider the corrections from the lepton side neglecting possible contributions from the mesons as they are neutral and much heavier than the leptons and the virtual corrections are therefore minimized compared with the lepton contribution [1]. The virtual corrections is then the sum of two separate terms

$$\delta^{\text{Virtual}} = \delta_{\Pi}^{\text{Virtual}} + \delta_{\text{vertex}}^{\text{Virtual}} ,$$

where $\delta_{\Pi}^{\text{Virtual}}$ denotes the contribution from the diagram in Fig. 2a called the vacuum-polarization correction and $\delta_{\text{vertex}}^{\text{Virtual}}$ is from the diagram in Fig. 2b and is called the correction to the QED vertex [7]. The vacuum-polarization diagram in Fig. 2a involves the insertion of a lepton loop which includes a pair of leptons being created and then annihilated [1]. Due to the mass of the ω meson, the invariant mass of the virtual photon is large enough for the on-shell production of hadronic particles as well as leptons, so both contributions need to be considered [1, 3]. The photon self-energy can then be written as

$$\Pi(q^2) = \Pi_{\text{L}}(q^2) + \Pi_{\text{H}}(q^2) , \tag{17}$$

where Π_{L} is the contribution from the lepton pair production and Π_{H} is from the hardonic contribution [5]. The total contribution from the vacuum polarization $\delta_{\Pi}^{\text{Virtual}}$ can then be written as [5]

$$\delta_{\Pi}^{\text{Virtual}}(x, y) = 2\text{Re}\{-\Pi(\Delta_M^2 x)\} .$$

The vacuum polarization insertion from the lepton loop Π_ℓ can be determined for a specific type of lepton ℓ in the loop using the expression

$$\Pi_\ell(\Delta_M^2 x) = \frac{\alpha}{\pi}\left\{\frac{8}{9} - \frac{\beta_\ell^2}{3} + \frac{\beta_\ell}{2}\left(1 - \frac{\beta_\ell^2}{3}\right)\log(-\gamma_\ell + i\epsilon)\right\} , \tag{18}$$

where β_ℓ and γ_ℓ are defined as [6]

$$\beta_\ell = \beta_\ell(x) = \sqrt{1 - \frac{4m_\ell^2}{\Delta_M^2 x}} , \quad \gamma_\ell \equiv \gamma_\ell(x) \equiv \frac{1 - \beta_\ell(x)}{1 + \beta_\ell(x)} . \tag{19}$$

Let us emphasize that the variables β_ℓ and γ_ℓ are related in form to the variables β and γ from Eqs. (7) and (8), but here they refer to leptons running in the virtual loops. The term $\log(-\gamma_\ell + i\epsilon)$ can be rewritten as $\log(-\gamma_\ell + i\epsilon) = \log\gamma_\ell + i\pi$. The total contribution from the leptons is then obtained by summing over the different species of leptons ℓ. For the ω meson decay we investigate, only the contributions from the electron and muon need to be considered, so the total contribution from lepton loops is

$$\Pi_{\rm L}(q^2) = \Pi_{\rm e}(q^2) + \Pi_{\mu}(q^2)\,. \tag{20}$$

The hadronic contribution, $\Pi_{\rm H}$, can be expressed as

$$\Pi_{\rm H}(q^2) = -\frac{q^2}{4\pi^2\alpha}\int_{4m_\pi^2}^{\infty}\frac{\sigma_{\rm H}(s')\mathrm{d}s'}{q^2 - s' + i\epsilon}\,, \tag{21}$$

where $\sigma_{\rm H}$ is the total cross section of the e^-e^+ annihilation reaction into hadrons. It can be determined by

$$\sigma_{\rm H}(q^2) = \frac{4\pi\alpha^2}{q^2}R(q^2)\,,$$

where $R(q^2)$ is ratio of the hadronic cross section in the e^-e^+ annihilation and the muon cross section with the data taken from the Particle Data Group [5, 3]. Now we need to evaluate the contribution from the vertex correction seen in Fig. 2b. This contribution can be written as

$$\delta^{\rm Virtual}_{\rm vertex}(x,y) = 2\,\mathrm{Re}\left\{F_1(\Delta_M^2 x) + \frac{2F_2(\Delta_M^2 x)}{1 + y^2 + \frac{\nu^2}{x}}\right\}.$$

The form factors $F_1(q^2)$ and $F_2(q^2)$ for the QED vertex corrections now need to be evaluated. The first F_1 is written as [6]

$$\begin{aligned} F_1(\Delta_M^2 x) = \frac{\alpha}{\pi}\Bigg\{-1 - \frac{1+2\beta^2}{4\beta}\log(-\gamma + i\epsilon) + \left[1 + \frac{1+\beta^2}{2\beta}\log(-\gamma+i\epsilon)\right]\log\frac{m}{\Lambda} \\ - \frac{1+\beta^2}{2\beta}[\mathrm{Li}_2(1-\gamma) + \frac{1}{4}\log^2(-\gamma+i\epsilon) - \frac{\pi^2}{4} - i\pi\log(1-\gamma)]\Bigg\}\,, \end{aligned} \tag{22}$$

where $\mathrm{Li}_2(z)$ is the dilogarithm function defined as $\mathrm{Li}_2(z) = \int_z^0 \mathrm{d}t\,\ln(1-t)/t$, γ is from Eq. (8), and Λ is the infrared cut-off denoting the lowest energy of the photon in the BS phenomenon [6]. For $\Lambda \to 0$ this introduces a singularity in the form of an IR divergence, so it acts as a regulator [6, 8]. The $F_2(q^2)$ term can be written as

$$F_2(\Delta_M^2 x) = \frac{\alpha}{\pi}\frac{\nu^2}{4x\beta}\log(-\gamma + i\epsilon)\,. \tag{23}$$

The total virtual correction can then be written as

$$\delta^{\rm Virtual}(x,y) = 2\,\mathrm{Re}\left\{-\Pi(\Delta_M^2 x) + F_1(\Delta_M^2 x) + \frac{2F_2(\Delta_M^2 x)}{1 + y^2 + \frac{\nu^2}{x}}\right\}. \tag{24}$$

We would also like to get virtual corrections without the y dependence. From Eq. (15) we find

$$\delta^{\rm Virtual}(x) = 2\,\mathrm{Re}\left\{-\Pi(\Delta_M^2 x) + F_1(\Delta_M^2 x) + \frac{3}{2}\frac{F_2(\Delta_M^2 x)}{1 + \frac{\nu^2}{2x}}\right\}. \tag{25}$$

If the whole geometric series for the one-loop insertions is summed over, this gives

$$\tilde{\Pi}(q^2) = -\frac{1}{1+\Pi(q^2)}\,.$$

Squaring the amplitude and then subtracting the LO part from this expression [6, 5] means that $\delta_{\Pi}^{\text{Virtual}}$ can be written as

$$\delta_{\Pi}^{\text{Virtual}}(x) = \frac{1}{|1+\Pi(\Delta_M^2 x)|^2} - 1\,. \tag{26}$$

This can then be used in Eq. (25) and replace the $2\text{Re}\{-\Pi(\Delta_M^2 x)\}$ term. Thus the total expression for δ^{Virtual} can then be written as

$$\delta^{\text{Virtual}}(x) = \frac{1}{|1+\Pi(\Delta_M^2 x)|^2} - 1 + 2\,\text{Re}\left\{F_1(\Delta_M^2 x) + \frac{3}{2}\frac{F_2(\Delta_M^2 x)}{1+\frac{\nu^2}{2x}}\right\}. \tag{27}$$

Now we need to consider the bremsstrahlung correction.

2.4 Bremsstrahlung Correction

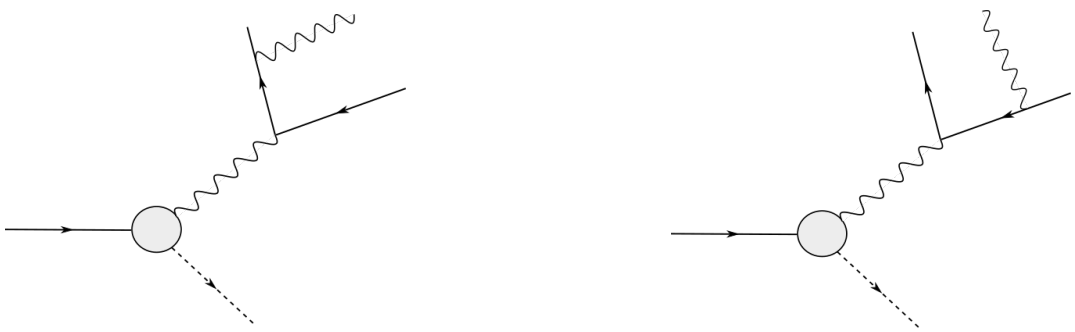

Figure 3: The bremsstrahlung correction diagrams at NLO in the QED expansion.

2.4.1 Total δ^{BS} Correction

The Feynman diagrams for the BS contribution can be seen in Fig. 3 and involve the emission of an BS photon from one of the leptons in the lepton pair. The treatment of the BS contribution builds of a similar discussion from Ref. [6]. The total contribution comes from including the effects from both diagrams, inclusive of their interference [1]. With the additional photon, the sum of the four-momenta involved in the decay are related by

$$p_1 = p_2 + q_1 + q_2 + k\,,$$

where k is now the four-momentum of the BS photon [6]. Similar to the virtual corrections, the BS from the mesons are also neglected due to the heavier mass of the mesons and the fact they are neutral which minimizes the BS correction [1]. The matrix element of this process is

$$i\mathcal{M}_{\text{BS}} = \frac{i^5 e^3}{(k+q_1+q_2)^2 + i\epsilon}\mathcal{F}_{\omega}\big((k+q_1+q_2)^2\big)\epsilon_{\mu\nu\alpha\beta}p_1^{\alpha}p_2^{\beta}\epsilon^{\mu}(\mathbf{p}_1)(\overline{u}(\mathbf{q}_1)I^{\nu\rho}v(\mathbf{q}_2))\epsilon_{\rho}^{*}(\mathbf{k})\,, \tag{28}$$

where $I^{\nu\rho}$ is defined as

$$I^{\nu\rho} = \gamma^\rho \frac{(\not{k} + \not{q}_1 + m)}{2k \cdot q_1 + i\epsilon}\gamma^\nu - \gamma^\nu \frac{(\not{k} + \not{q}_2 - m)}{2k \cdot q_2 + i\epsilon}\gamma^\rho \,. \tag{29}$$

A new variable can now also be introduced called $s_\gamma = (k + p_2)^2$ [6] which in this case is the invariant mass squared of the BS photon and the π^0 meson. For the full matrix element squared $\overline{|\mathcal{M}_{\text{BS}}|^2}$, the result is not written out here due to its long nature. The BS contribution to the differential decay width can be written as

$$\frac{\mathrm{d}^2\Gamma^{\text{NLO}}_{\text{BS}}(x,y)}{\mathrm{d}x\mathrm{d}y} = \frac{1}{2m_\omega}\frac{\pi^3\Delta_M^2\lambda^{\frac{1}{2}}(x)}{16(2\pi)^8 m_\omega^2}\int J\left[\overline{|\mathcal{M}_{\text{BS}}|^2}\right]\mathrm{d}s_\gamma \,. \tag{30}$$

The differential decay width can also be integrated over y to yield $\mathrm{d}\Gamma^{\text{NLO}}_{\text{BS}}(x)/\mathrm{d}x$. Above J is an operator that acts on an arbitrary invariant function $f(k, p_2)$ and is defined as

$$J\left[f(k,p_2)\right] = \frac{1}{2\pi}\int \frac{\mathrm{d}^3k}{k_0}\frac{\mathrm{d}^3p_2}{p_{2,0}} f(k,p_2)\delta^{(4)}(p_1 - q_1 - q_2 - p_2 - k)\,, \tag{31}$$

where $\delta^{(4)}$ is the Dirac delta function [6]. This expression can be rewritten by introducing a reference system where $\mathbf{p}_1 - \mathbf{q}_1 - \mathbf{q}_2 = 0$. This then means that $\mathbf{p}_2 = -\mathbf{k}$. The photon and pion are also assumed to be on the mass shell such that $k^2 = 0$ and $p_2^2 = m_\pi^2$. Rewriting J then gives

$$J\left[f(k,p_2)\right] = \frac{1}{4\pi}\frac{\tilde{\omega}}{\omega}\int \mathrm{d}\Omega_{\mathbf{k}}\, f(k,\tilde{p_2})\big|_{|\mathbf{k}|=\frac{\tilde{\omega}}{2}} \,. \tag{32}$$

Here ω refers to a new variable defined as $\omega = \sqrt{s_\gamma}$, $\tilde{\omega}$ is defined as $\tilde{\omega} = (s_\gamma - m_\pi^2)/\sqrt{s_\gamma}$, and finally $\tilde{p}_2$ denotes the four-momentum of the π^0 meson such that $\tilde{p}_2$ has components $\tilde{p}_2 = (p_{2,0}, -\mathbf{k})$. The total BS correction $\delta^{\text{BS}}(x,y)$ is then determined from Eq. (14)

$$\delta^{\text{BS}}(x,y) = \frac{\mathrm{d}^2\Gamma^{\text{NLO}}_{\text{BS}}(x,y)}{\mathrm{d}x\mathrm{d}y}\Bigg/\frac{\mathrm{d}^2\Gamma^{\text{LO}}(x,y)}{\mathrm{d}x\mathrm{d}y} \,. \tag{33}$$

Hence we need to determine the NLO differential decay width $\mathrm{d}^2\Gamma^{\text{NLO}}/\mathrm{d}x\mathrm{d}y$ from Eq. (30). To do this the term $J\left[\overline{|\mathcal{M}_{\text{BS}}|^2}\right]$ has to be evaluated. When it comes to the matrix element squared $\overline{|\mathcal{M}_{\text{BS}}|^2}$, there are a couple of other definitions that are useful to introduce when dealing with the operator J. We write

$$A \equiv k \cdot q_2 \,, \tag{34}$$
$$B \equiv k \cdot q_1 \,, \tag{35}$$
$$E \equiv (k + q_1 + q_2)^2 \,, \tag{36}$$

where E can be related to A and B as

$$E = \Delta_M^2 x + 2A + 2B \,. \tag{37}$$

When the operator J is then applied on the matrix element squared, the integral contained in J acting on combinations of these kinematic variables need to be considered. Eq. (30) also includes integrating over s_γ. To go beyond the soft-photon approximation the full range of s_γ values need to be evaluated. When examining $\overline{|\mathcal{M}_{\text{BS}}|^2}$ it turns out that there

are multiple terms that include A, B, and E that become divergent when integrated over the full range of s_γ. One way that we could then split matrix element squared $\overline{|\mathcal{M}_{\rm BS}|^2}$ is into convergent and divergent parts such that

$$\overline{|\mathcal{M}_{\rm BS}|^2} = \overline{|\mathcal{M}_{\rm BS}|^2}\Big|_{\rm Conv.} + \overline{|\mathcal{M}_{\rm BS}|^2}\Big|_{\rm Div.}\,, \tag{38}$$

where $\overline{|\mathcal{M}_{\rm BS}|^2}\big|_{\rm Conv.}$ denotes the IR convergent part of the matrix element squared and $\overline{|\mathcal{M}_{\rm BS}|^2}\big|_{\rm Div.}$ denotes the divergent part [6]. This type of splitting is in principle not unique, but in our approach this split emerges naturally and can be defined properly in this way even if it is not unique. We then need to evaluate these terms separately and combine them after integrating over s_γ to give the full $J\left[\overline{|\mathcal{M}_{\rm BS}|^2}\right]$ term.

2.4.2 The Convergent $\delta^{\rm BS}$ Correction

The IR convergent part $\overline{|\mathcal{M}_{\rm BS}|^2}\big|_{\rm Conv.}$ contains several terms with combinations of A, B, and E. The $\overline{|\mathcal{M}_{\rm BS}|^2}\big|_{\rm Conv.}$ term can also be split further into two parts that are equivalent under the exchange of $q_1 \leftrightarrow q_2$ [6]. The effect of J acting on one half of these terms can be seen in Appendix A. The other half of J acting on $\overline{|\mathcal{M}_{\rm BS}|^2}\big|_{\rm Conv.}$ can then be gained by exchanging $\Delta_m^2 \leftrightarrow -\Delta_m^2$ [6]. Adding both of these contributions then gives the total $J\left[\overline{|\mathcal{M}_{\rm BS}|^2}\big|_{\rm Conv.}\right]$. Integrating this term over s_γ requires considering the integration limits on s_γ. The minimum value for s_γ ($s_\gamma^{\rm min}$) would be when $|\vec{k}| = 0$ such that $s_\gamma^{\rm min}$ is simply the mass squared of the π^0 meson. This then means we can write $s_\gamma^{\rm min} = m_\pi^2$. The upper integration limit $s_\gamma^{\rm max}$, however, will take the shape

$$s_\gamma^{\rm max} = m_\omega^2 + \Delta_M^2 x - \sqrt{4m_\omega^2\Delta_M^2 x + \frac{(\Delta_m^2)^2}{\beta^2}}\,. \tag{39}$$

2.4.3 The Divergent $\delta^{\rm BS}$ Correction

The divergent part $\overline{|\mathcal{M}_{\rm BS}|^2}\big|_{\rm Div.}$ can be written as

$$\overline{|\mathcal{M}_{\rm BS}|^2}\Big|_{\rm Div.} = 4\alpha\pi\left[s\left(1-\frac{2m^2}{s}\right)\frac{1}{AB} - m^2\left(\frac{1}{A^2}+\frac{1}{B^2}\right)\right]\overline{|\mathcal{M}_{\rm LO}|^2}\,, \tag{40}$$

where $\overline{|\mathcal{M}_{\rm LO}|^2}$ is the matrix element squared for LO diagram. Due to the integral over s_γ being divergent the total integral $\int J\left[\overline{|\mathcal{M}_{\rm BS}|^2}\big|_{\rm Div.}\right]\mathrm{d}s_\gamma$ has to be done analytically to deal with the singularity. To do this using Eq. (32) is no longer appropriate to simplify the integrals and another approach has to be taken using Eq. (31). This includes doing integrals over the $1/A^2$, $1/B^2$, and $1/AB$ terms as seen in Eq. (40). Starting from considering $J\left[1/AB\right]$ a new expression for the integral can be derived. This gives

$$J\left[\frac{1}{AB}\right] = 4\int_0^1\int_{s_\gamma^{\rm min}}^{s_\gamma^{\rm max}} \frac{\sqrt{\lambda(s_\gamma, m_\pi^2, \Lambda^2)}}{\lambda(s_\gamma, m_\pi^2, \Lambda^2)(A_1^2 - A_2^2) + 4s_\gamma\Lambda^2 A_1^2}\,\mathrm{d}s_\gamma\mathrm{d}u\,, \tag{41}$$

where $A_1 = [uq_{2,0} + (1-u)q_{1,0}]$ and $A_2 = |u\boldsymbol{q_2} + (1-u)\boldsymbol{q_1}|$, $A_1^2 - A_2^2 = m^2 + u(1-u)(s-4m^2)$, and $4s_\gamma\Lambda^2 A_1^2 = \frac{1}{4}[m_\omega^2 - s - s_\gamma + (2u-1)\Delta_m^2]$. Here the integral over u comes from using Feynman parametrization in the derivation and Λ is the same photon-mass regulator as

used in Eq. (22). The full derivation of this expression can be seen in Appendix B. This integral then needs to be performed over s_γ. To simplify the integral, the limit $\lim_{\Lambda\to 0}$ is carefully considered whenever possible and the full range of the approximation and integral is given in Appendix C. The full expression is then

$$J\left[\frac{1}{AB}\right] = \int_0^1 \frac{4}{V}\left(\log\frac{s_\gamma^{\max}-m_\pi^2}{m\,m_\pi}+\log\frac{m}{\Lambda}\right) - \frac{4}{VH}\operatorname{atanh} H\,\mathrm{d}u\,. \tag{42}$$

Here V and H are variables introduced for convenience and are defined as

$$V = m^2 + (s-4m^2)(1-u)u\,, \tag{43}$$

$$H = \sqrt{1-\frac{16m_\pi^2 V}{4Q}}\,, \tag{44}$$

where Q is defined as

$$Q = \frac{1}{4}(M_\omega^2 - s - m_\pi^2 + (2u-1)\Delta_m^2)^2\,.$$

Here it can be seen that the only remaining divergent term is $\log m/\Lambda$ as Λ approaches zero. We can then get the other terms $J\left[1/A^2\right]$ and $J\left[1/B^2\right]$ by setting $u=1$ and $u=0$ respectively in Eq. (42) as seen from using the definitions in Appendix B. The different terms of the divergent correction then become

$$J\left[\frac{1}{A^2}\right] = \frac{4}{m^2}\left(\log\frac{s_\gamma^{\max}-m_\pi^2}{m\,m_\pi}+\log\frac{m}{\Lambda}\right) - \frac{4}{m^2 H_1}\operatorname{atanh} H_1\,, \tag{45}$$

$$J\left[\frac{1}{B^2}\right] = \frac{4}{m^2}\left(\log\frac{s_\gamma^{\max}-m_\pi^2}{m\,m_\pi}+\log\frac{m}{\Lambda}\right) - \frac{4}{m^2 H_0}\operatorname{atanh} H_0\,, \tag{46}$$

$$J\left[\frac{1}{AB}\right] = \int_0^1 \frac{4}{V}\left(\log\frac{s_\gamma^{\max}-m_\pi^2}{m\,m_\pi}+\log\frac{m}{\Lambda}\right) - \frac{4}{VH}\operatorname{atanh} H\,\mathrm{d}u\,, \tag{47}$$

where new definitions H_1 and H_0 for $u=1$ and $u=0$ respectively are introduced for convenience

$$H_{1,0} = \sqrt{1-\frac{16m_\pi^2 m^2}{4Q_{1,0}}}\,, \tag{48}$$

where Q_1 and Q_0 are defined as

$$Q_{1,0} = \frac{1}{4}(M_\omega^2 - s - m_\pi^2 \pm \Delta_m^2)^2\,. \tag{49}$$

The integral over u for the $1/AB$ term can be evaluated further over the first term to give

$$\int_0^1 \frac{4}{V}\left(\log\frac{s_\gamma^{\max}-m_\pi^2}{m\,m_\pi}+\log\frac{m}{\Lambda}\right)\mathrm{d}u = -\frac{8}{\Delta_M^2 x\beta}\log\gamma\left(\log\frac{s_\gamma^{\max}-m_\pi^2}{m\,m_\pi}+\log\frac{m}{\Lambda}\right). \tag{50}$$

The full integral of $J\left[1/AB\right]$ can be seen in Appendix C. So a final expression for $J\left[1/AB\right]$ is then

$$J\left[\frac{1}{AB}\right] = -\frac{8}{\Delta_M^2 x\beta}\log\gamma\left(\log\frac{s_\gamma^{\max}-m_\pi^2}{m\,m_\pi}+\log\frac{m}{\Lambda}\right) - \int_0^1 \frac{4}{VH}\operatorname{atanh} H\,\mathrm{d}u\,. \tag{51}$$

The remaining integral over u is left unresolved as no analytical solution was found as of the time of writing and no full analytical solution is believed to exist either. This remaining integral over u then has to be performed numerically to give the full expression. The total expression for the divergent part of δ^{BS} is then gained by inserting the results back into Eq. (30). We can use Eq. (33) to get the value for $\delta^{\mathrm{BS}}(x, y)$. By integrating over the full range of s_γ the calculation for the complete BS correction then by definition goes beyond the soft-photon approximation. The BS expressions can also be integrated over y to yield $\delta^{\mathrm{BS}}(x)$. The total correction to the differential decay width is then given by simply adding the virtual and BS correction ($\delta^{\mathrm{Virtual}}$ and δ^{BS}) corrections.

2.4.4 Soft-photon Approximation

It is worth taking a quick detour to compare how our approach differs with the soft-photon approximation. In the soft-photon approximation, the four-momentum k of the BS photon in the matrix element in Eq. (29) is systematically assumed to go towards zero. Thus, when considering the matrix element squared in Eq. (39), the convergent part $\overline{|\mathcal{M}_{\mathrm{BS}}|^2}\Big|_{\mathrm{Conv.}}$ will disappear. However, the divergent matrix element squared would still need to be considered. So, in the soft-photon approximation the radiative correction is the sum of the correction stemming from the divergent part of the bremsstrahlung matrix element squared and the virtual correction. In this approximation, the correction becomes form-factor-independent. This is due to that the correction $\delta^{\mathrm{BS}}(x, y)$ is calculated from dividing the NLO BS differential decay width and the LO differential decay width which in this limit cancels the form factor.

By construction, the soft-photon approximation becomes exact as the energy of the bremsstrahlung photon vanishes. Thus, within this approximation, we can obtain physically relevant results when only soft-photons are considered. In this regard, we can introduce $s_\gamma^{\mathrm{Cutoff}}$ defined as $s_\gamma^{\mathrm{Cutoff}} = (m_\pi + \epsilon)^2$ where ϵ is some constant term. This cutoff then signifies the energy above which the emitted BS photons have been left out. When using s_γ^{max} in Eq. (51), this would then be replaced by either $s_\gamma^{\mathrm{Cutoff}}$ or s_γ^{max} depending on which is the smaller term. This type of correction is then called the soft-photon bremsstrahlung (in the soft-photon approximation). The size of the BS corrections beyond the soft-photon approximation with hard photons included, however, depends on the type of form-factor model used, which we now need to specify.

2.5 Form Factor Models

There are numerous different approaches that try to model the electromagnetic form factors based on different assumptions and ideas. For this thesis, four different models were used: the vector-meson-dominance (VMD) model [9, 10], lowest-meson-dominance (LMD) model [11], tree-level (TL) model [10], and the two-hadron-saturation (THS) model [7]. In the simple VMD ansatz, the pole structure is assumed to be solely given by the exchange of vector resonances [9, 10]. This allows us to write the correlator of the pion and two vector currents (with virtualities p^2 and q^2) as

$$\mathcal{F}_{\mathrm{VMD}}(p^2, q^2) = -\frac{N_C}{8\pi^2 F} \frac{M_V^4}{(p^2 - M_V^2)(q^2 - M_V^2)}\,, \tag{52}$$

where M_V is the mass of the ground-state vector-meson multiplet approximately given by the mass of the ρ meson for this ω decay, N_C is the number of colors ($N_C = 3$ in QCD), and F is the pion decay constant.

Then, by fixing one of the virtualities to the ω mass, we have in general for the form factor

$$\mathcal{F}(q^2) = \lim_{p^2 \to M_V^2} \frac{1}{Z_\omega}(p^2 - M_V^2)\mathcal{F}(p^2, q^2)\,, \tag{53}$$

where Z_ω is related to the overlap between the ω meson and the vector quark current [7]. This limit is then performed for all the form factors considered and the normalized form factor $\hat{\mathcal{F}}(q^2) = \mathcal{F}(q^2)/\mathcal{F}(0)$ is obtained. We can then write the normalized form factor squared for the VMD model $|\hat{\mathcal{F}}_{\rm VMD}(q^2)|^2$ as

$$|\hat{\mathcal{F}}_{\rm VMD}(q^2)|^2 = \left|\frac{\mathcal{F}_{\rm VMD}(q^2)^2}{\mathcal{F}_{\rm VMD}(0)^2}\right| = \frac{M_V^4}{(q^2 - M_V^2)^2}\,. \tag{54}$$

An alternative for the VMD form factor is the pole approximation written as

$$|\hat{\mathcal{F}}(q^2)|^2 = \left(1 - \frac{q^2}{\Lambda^2}\right)^{-2}\,, \tag{55}$$

where Λ is the effective mass of the virtual vector meson and Λ^{-2} is related to the transition FF slope at $q^2 = 0$ [4] derived from experimental data. For the LMD model, it assumes that the lowest-lying multiplet of the pseudoscalar and vector resonances are considered when deriving its form and that these are enough to capture the main contribution [11]. In this approach the correlator becomes

$$\mathcal{F}_{\rm LMD}(p^2, q^2) = \mathcal{F}_{\rm VMD}(p^2, q^2)\left(1 - \frac{4\pi^2 F^2(p^2 + q^2)}{N_C M_V^4}\right). \tag{56}$$

The normalized form factor squared then becomes

$$|\hat{\mathcal{F}}_{\rm LMD}(q^2)|^2 = |\hat{\mathcal{F}}_{\rm VMD}(q^2)|^2 \cdot \left(\frac{1 - \frac{4\pi^2 F^2(M_V^2 + q^2)}{N_C M_V^4}}{1 - \frac{4\pi^2 F^2}{N_C M_V^2}}\right)^2. \tag{57}$$

The TL model involves introducing a tree-level diagram of the NLO contributions when considering the Lagrangian for this type of decay. This introduces another constant contact term which adjusts the VMD model form seen in Eq. (53) [10]. This leads to the form factor that can be written as

$$\mathcal{F}_{\rm TL}(q^2) = \mathcal{F}_{\rm TL}(0)\frac{M_V^2 + q^2}{M_V^2 - q^2}\,, \tag{58}$$

where M_V again is the mass of the virtual vector meson. The TL normalized form factor squared then takes the shape

$$|\hat{\mathcal{F}}_{\rm TL}(q^2)|^2 = \left(\frac{M_V^2 + q^2}{M_V^2 - q^2}\right)^2. \tag{59}$$

Finally, the THS model is considered. In this approach, it is similar to LMD but expands on it and introduces two vector meson resonances with masses M_{V_1} and M_{V_2} [7]. In this model, the correlator can be written as

$$\begin{aligned}\mathcal{F}_{\rm THS}(p^2, q^2) = &-\frac{N_C}{8\pi^2 F}\frac{M_{V_1}^4 M_{V_2}^4}{(p^2 - M_{V_1}^2)(p^2 - M_{V_2}^2)(q^2 - M_{V_1}^2)(q^2 - M_{V_2}^2)} \\ &\times\left[1 + \frac{\kappa}{2N_C}\frac{p^2 q^2}{(4\pi F)^4} - \frac{4\pi^2 F^2(p^2 + q^2)}{N_C M_{V_1}^2 M_{V_2}^2}\left(6 + \frac{p^2 q^2}{M_{V_1}^2 M_{V_2}^2}\right)\right],\end{aligned} \tag{60}$$

where κ is a free dimensionless parameter of the model that needs to be fitted from experimental data. It is expected to lie in the interval $(-45, 30)$ and was found to be as high as 21 in Ref. [7]. The normalized form factor squared becomes

$$|\hat{\mathcal{F}}_{\text{THS}}(q^2)|^2 = \frac{M_{V_1}^4 M_{V_2}^4}{(q^2 - M_{V_1}^2)^2 (q^2 - M_{V_2}^2)^2} \left| \frac{\left(1 + \frac{\kappa}{2N_C} \frac{M_{V_1}^2 q^2}{(4\pi F)^4} - \frac{4\pi^2 F^2 (M_{V_1}^2 + q^2)}{N_C M_{V_1}^2 M_{V_2}^2} \left(6 + \frac{M_{V_1}^2 q^2}{M_{V_1}^2 M_{V_2}^2}\right)\right)}{\left(1 - \frac{24\pi^2 F^2}{N_C M_{V_2}^2}\right)} \right|^2 . \tag{61}$$

The mass M_{V_2} is taken in the interval $M_{V_2} \in [1400, 1740]$ MeV, i.e. between the masses of the first and second physical excitations, while the mass M_{V_1} will, for the ω decay, approximately be given by the mass of the ρ meson [7]. More details on the mentioned form-factor models can be found in Refs. [9], [11], [10], and [7]. Now, by using the normalized form-factor models in the expressions for the BS, we can then determine the total correction.

3 Method and Implementation

3.1 Implementing the δ^{Virtual} and δ^{BS} Corrections

With the results for the virtual and the BS corrections in hand, the full correction δ to the differential decay width can be determined. To do this they once again need to be treated separately. For the virtual correction (δ^{Virtual}), Eq. (27) fully determines the correction using the definitions for the form factors from Eq. (22) and Eq. (23). The hadronic contribution stems from integrating over the experimental data on R using Eq. (21). These numerical results were calculated using Wolfram Mathematica which was subsequently used for implementing all the expressions used in the thesis.

For the BS contribution to the overall correction δ^{BS}, the convergent and divergent parts of the matrix element squared have to be treated separately as well when implementing. To calculate the $\delta^{\text{BS}}(x)$ the convergent matrix element squared was numerically integrated over s_γ using the interval $[s_\gamma^{\min}, s_\gamma^{\max}]$ with Eq. (39) for $s_\gamma^{\max}$ but was also numerically integrated over y using the interval $[-\beta, \beta]$. For the divergent contribution the value for $s_\gamma^{\max}$ is used in Eq. (45), Eq. (46), and Eq. (51) while in Eq. (51) the numerical integral over u is performed. The results were then inserted back into Eq. (30) and finally integrated numerically over y.

Combining the results from both the convergent and divergent contributions and using the results from Eq. (12) the total BS correction is determined numerically. When introducing the form factor models into the overall matrix element squared, an ansatz was used for writing a general normalized form factor squared as

$$|\hat{\mathcal{F}}(q^2)|^2 = \delta_0 + \delta_1 \frac{M_V^2}{q^2 - M_V^2} + \delta_2 \frac{M_V^4}{(q^2 - M_V^2)^2} , \tag{62}$$

which is a convenient form suitable for the integrals involved. The δ_i in this equation are coefficients that make the specific form factor model used fit into the ansatz and M_V^2 can also vary. This allows us to perform one analytical calculation and then the appropriate form factor model can be chosen by using the suitable δ_i and M_V^2 terms. This ansatz might need to be used repeatedly for more complicated form factor models such as the

THS model, where two consecutive calculations have to be performed to fit the model into the ansatz due to multiple resonance masses involved. The list of δ_i terms and M_V^2 can be seen in Appendix D. For comparison, the result for only the divergent matrix element squared and the virtual corrections were added to show the soft-photon approximation. An example of the soft-photon bremsstrahlung approach was then calculated using that $s_\gamma^{\max}$ was set equal to $\min(s_\gamma^{\max}, s_\gamma^{\text{Cutoff}})$. Specifically in this thesis, $\epsilon = 5\,\text{MeV}$ was used.

3.2 Full Correction and Experimental Data

When the two different contributions δ^{Virtual} and δ^{BS} are added together the IR divergence terms in Eq. (22), Eq. (45), Eq. (46), and Eq. (51) will cancel, leaving the calculation finite. This also gives the total correction that can be used in Eq. (1) to extract the form factor. The experimental data on the form factors for the ω decay were taken from four different experiments called the NA60(p-A), NA60(In-In), Lepton-G, and A2. All the different experiments except the A2 use the muon channel to measure the form factor while the A2 uses the electron channel [12, 13, 14, 15]. To apply the radiative corrections to the differential decay width and get a new estimate for the form factor squared, we have to consider how the form factor was determined from the experimental data. From Eq. (1) we know that the estimate for the form factor should be the ratio $\frac{\mathrm{d}\Gamma}{\mathrm{d}q^2} / \frac{\mathrm{d}\Gamma}{\mathrm{d}q^2}|_{\text{Point}}$. Since the original experiments did not consider the radiative corrections when calculating $\mathrm{d}\Gamma/\mathrm{d}q^2|_{\text{Point}}$, this suggests that $\mathrm{d}\Gamma/\mathrm{d}q^2|_{\text{Point}}$ is simply the LO differential decay width. This then means that the data for the FF in the experiments are really

$$\frac{\mathrm{d}\Gamma(x)}{\mathrm{d}x} \Big/ \frac{\mathrm{d}\Gamma^{\text{LO}}(x)}{\mathrm{d}x} = [1 + \delta(x)]\, |\hat{\mathcal{F}}_\omega(x\Delta_M^2)|^2 \,.$$

Thus in order to get a new estimate for the form factor squared we need to divide through by $[1 + \delta]$ such that

$$|\hat{\mathcal{F}}_\omega(x\Delta_M^2)|^2_{\text{New}} = \frac{|\hat{\mathcal{F}}_\omega(x\Delta_M^2)|^2_{\text{Measured}}}{[1 + \delta(x)]} \,. \tag{63}$$

As a result, applying this formula to the different data sets we get the new estimates for the normalized form factor squared. When dealing with the A2 data set the electron mass has to be used for the lepton mass when computing the correction δ. For the other data sets the muon mass has to be used to compute the corrections. If the THS model is to be used for computing the correction, the free parameter κ needs to be fitted from experimental data on the form factor [7]. Using the data from the four experiments, the THS model was used to fit the data and κ was found to be $\kappa = 20.6 \pm 1.7$. However, the last three data points in the total set are often not trusted. As a consequence these data points can be rejected and a new fit can be done. The new κ was then found to be $\kappa = 19.5 \pm 1.5$. Using this adjusted κ value the total correction was then performed. Another parameter that was fitted is the Λ^{-2} term in Eq. (55). This was done for the corrected data set and then compared with the uncorrected data fits in Refs. [14], [12], and [15].

4 Results

4.1 Total Correction for e and μ Channels

The total correction $\delta(x)$ was computed for the different form factor models outlined in Section 2.5. This was done for both the electron and muon channels as seen in Figs. 4a and 4b, respectively, and both the divergent matrix element squared added to the virtual corrections as well as the soft-photon bremsstrahlung.[1] In Fig. 4, the TL form factor model has the largest magnitude correction compared to the other form factor models in both channels. The THS model passes below the TL model in both channels but is still larger in magnitude than both the LMD and VMD models corrections. The corrections for the LMD model on the other hand are the lowest in magnitude of all the models. The VMD and LMD models are bunched closely together but the LMD here passes below the VMD model at all points. The overall corrections do, ultimately, align closely for all the different form factor models, converging in both channels for large and small x. This suggests that the overall correction is model-independent to an extent. The two channels do show significant different behavior. The electron channel correction quickly becomes negative after remaining positive over the range $x \in [\nu^2, 0.2]$. The muon channel on the other hand remains positive over the range $x \in [\nu^2, 0.78]$. Both channels become sharply negative as x approaches 1. We then find that for larger lepton masses the magnitude of the correction depends on the mass of the lepton, with the muon showing a lower magnitude correction compared with the electron correction. Both channels show a significant deviation as x approaches ν^2. This comes from the EM form factor F_1 in Eq. (22) and is connected to the Coulomb self-interaction of the leptons at the threshold and is an integrable divergence.

4.2 Form Factor Data Correction

The result of plotting the uncorrected data points with the different form factor models are seen in Fig. 5. The THS model for the adjusted data set with $\kappa = 19.5 \pm 1.5$ and the non-adjusted with $\kappa = 20.6 \pm 1.7$ are plotted with the other form factors in Fig. 5 with error bands plotted as well. The different THS models show significant overlap. The deviation of the data compared to the theoretical models is readily apparent here as neither form factor model is fully able to fit the entire set of the data. The corrections were then calculated using the THS model using the adjusted value for the κ for each respective data set. The electron channel was used for the A2 data and the muon channel for the other data sets. The result of corrections can be seen in Fig. 6.

It is worth looking closer at the A2 data set and its correction as seen in Fig. 7. This illustrates that although it might not be visible in Fig. 6b, when looking over the full range of the plot ultimately the lower $\sqrt{q^2}$ values do demonstrate the size of the correction of a few percentage points. The other graphs showed similar detail but was far less visible and are not included here.

[1] The numerical values used in the calculations were $m_\omega = 782.65\,\text{MeV}$, $m_\pi = 134.9766\,\text{MeV}$, $m_e = 0.510999\,\text{MeV}$, $m_\mu = 105.658\,\text{MeV}$, and $\alpha = 1/137.036$.

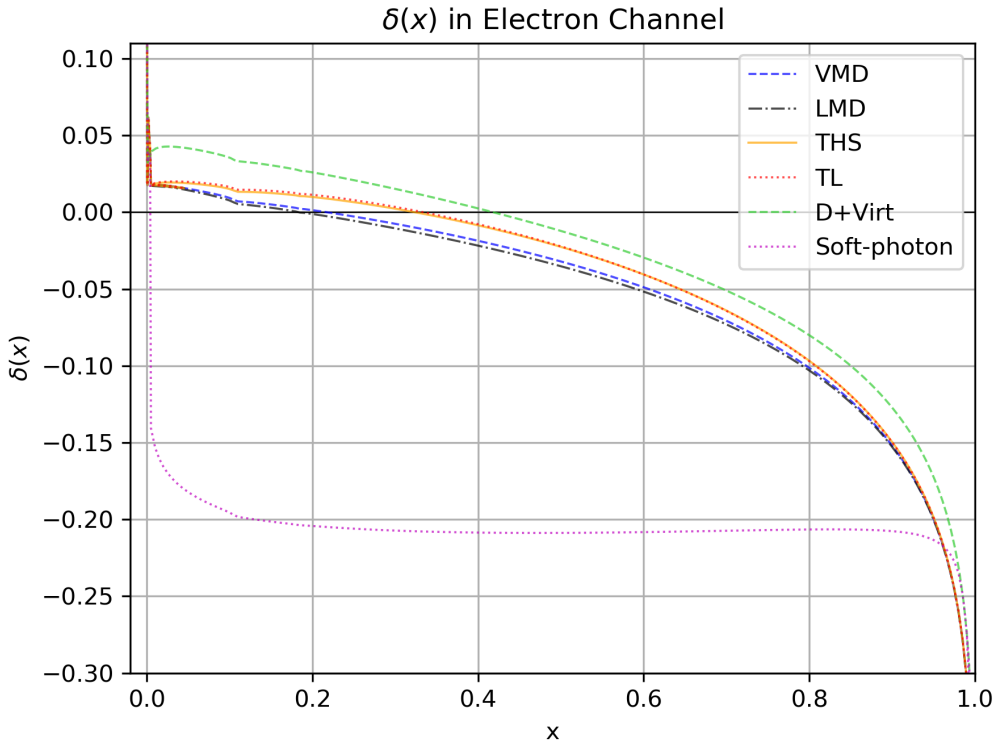

(a) Electron Channel

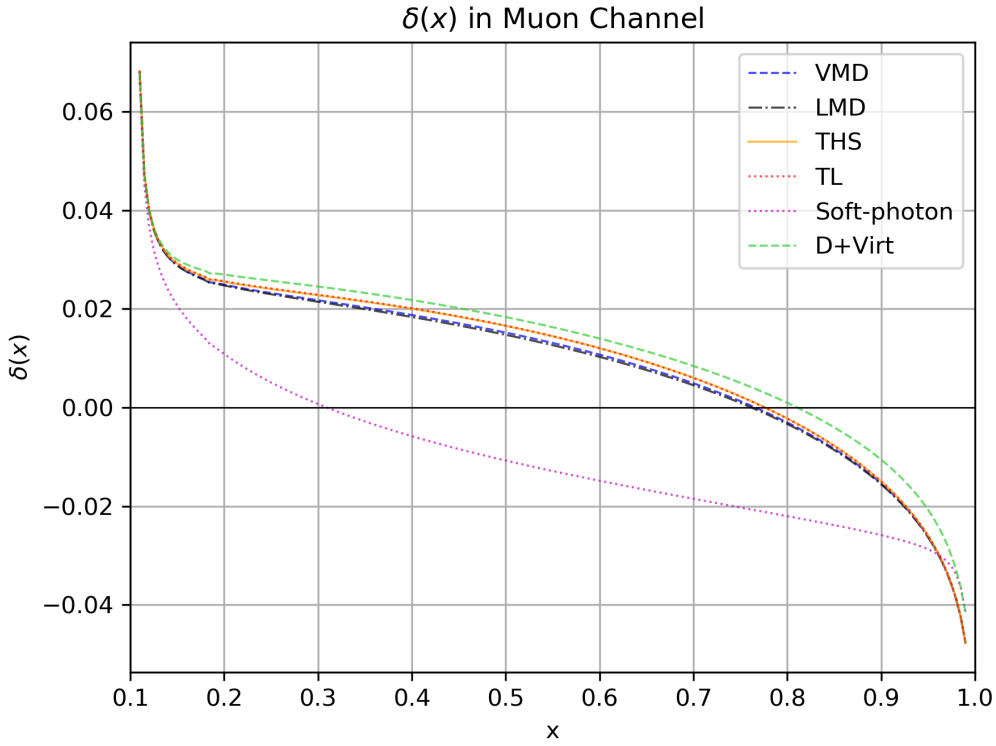

(b) Muon Channel

Figure 4: The total correction for the electron and muon channels. The correction for each specific form factor model is included in conjunction with the soft-photon approximation with the divergent part of the matrix element squared added to the virtual corrections (D+Virt), and the soft-photon bremsstrahlung with s_γ^{Cutoff} using $\epsilon = 5\,\text{MeV}$.

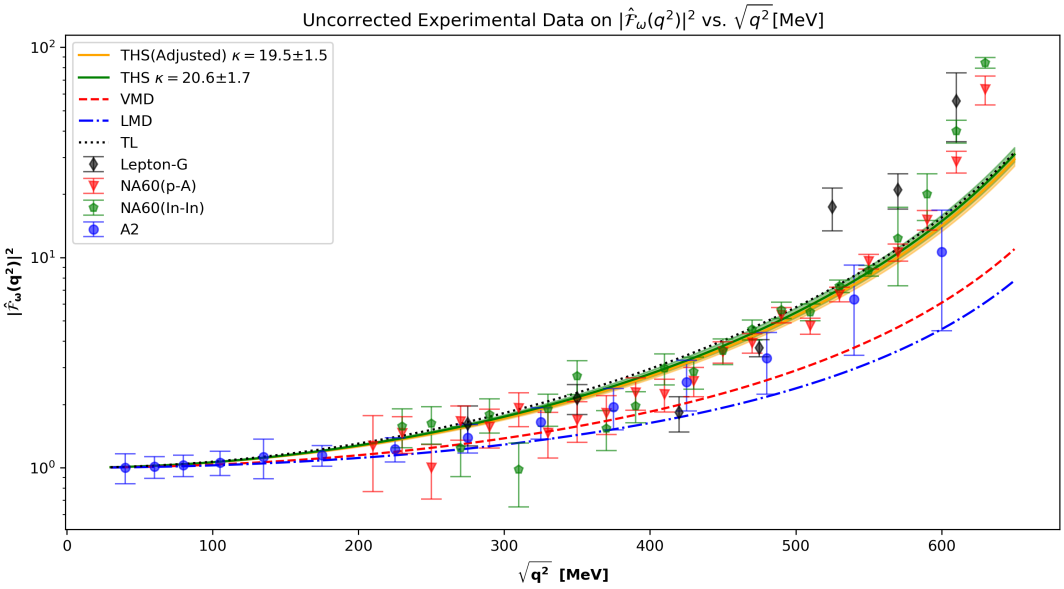

Figure 5: The uncorrected data with adjusted and non-adjusted κ plotted. The uncorrected data points from the four separate experiments with the four different form factor models $|\hat{\mathcal{F}}_\omega(q^2)|^2$ are plotted. The adjusted THS model with $\kappa = 19.5 \pm 1.5$ and its associated error band and the non-adjusted THS model with $\kappa = 20.6 \pm 1.7$ and its associated error band were also plotted.

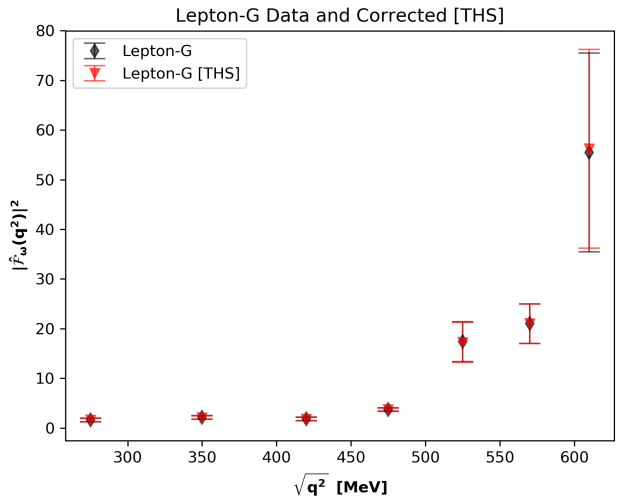

(a) Corrected Lepton-G data.

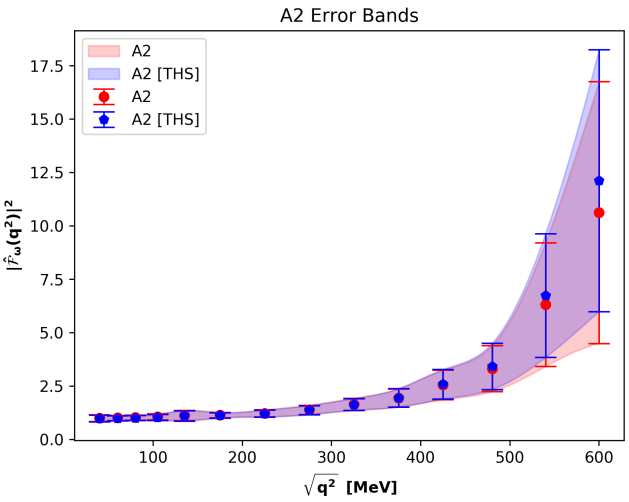

(b) Corrected A2 data and continuous error bands.

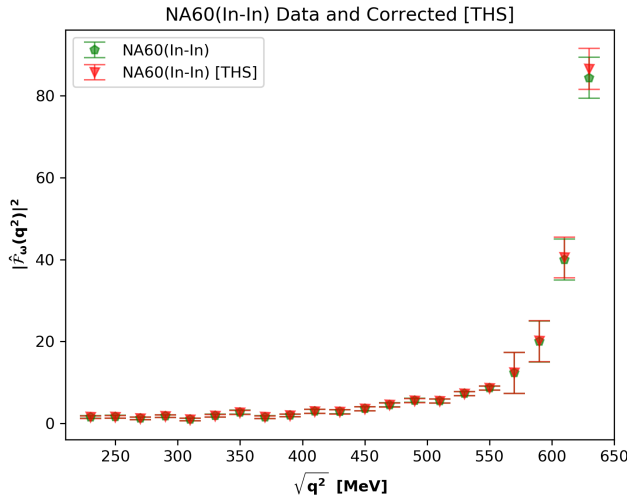

(c) Corrected NA60(In-In) data.

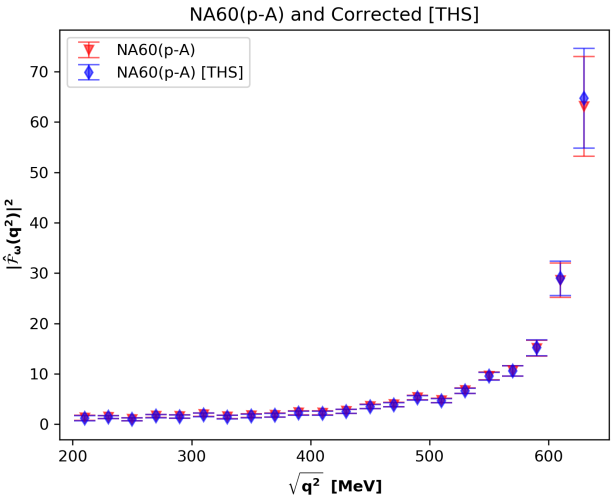

(d) Corrected NA60(p - A) data.

Figure 6: The corrected and uncorrected data. The corrections were performed using the adjusted THS model value for the κ. The A2 figure had its error bands plotted for the uncorrected vs. corrected data.

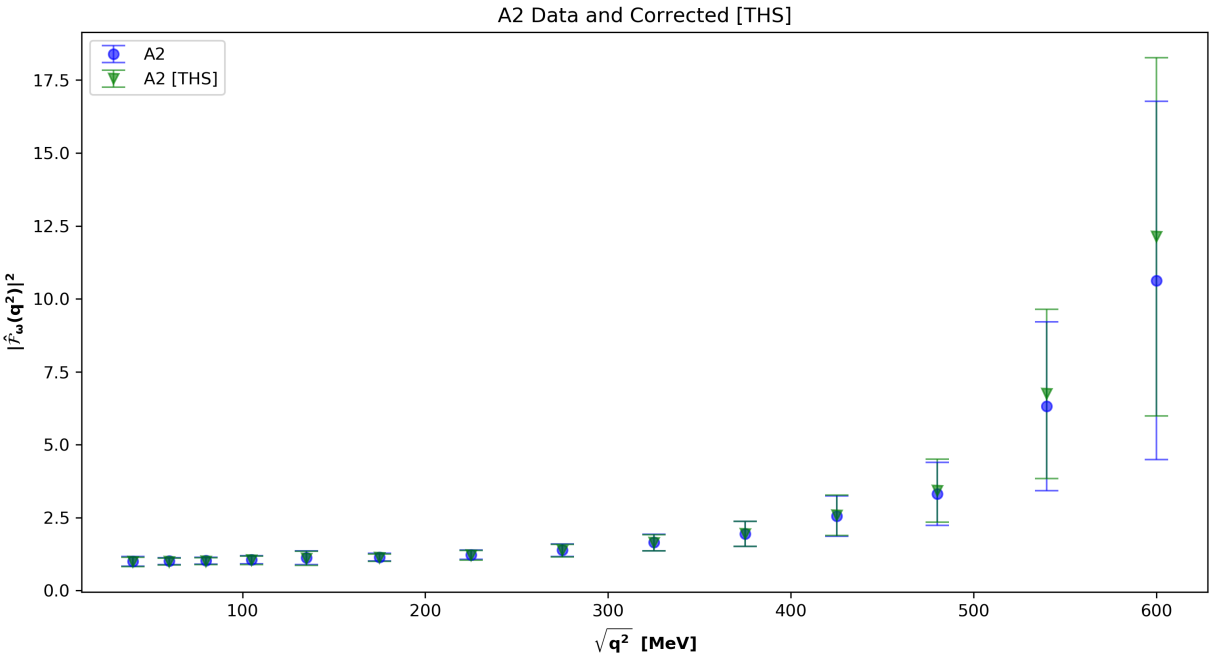

(a) A2 data over full range of data.

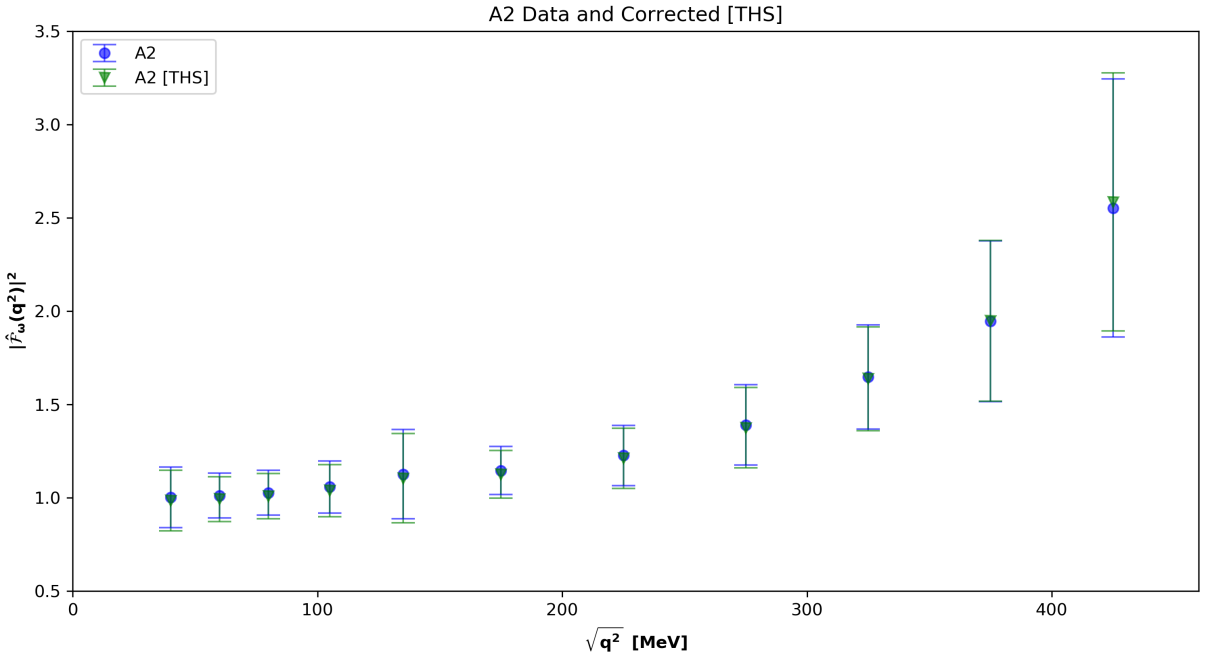

(b) A2 data over the range $\sqrt{q^2} \in [40, 450]\,\text{MeV}$.

Figure 7: The A2 data corrected using the THS model. The full range of the data and a limited range ($\sqrt{q^2} \in [40, 450]\,\text{MeV}$) are shown in the subfigures (a) and (b) respectively.

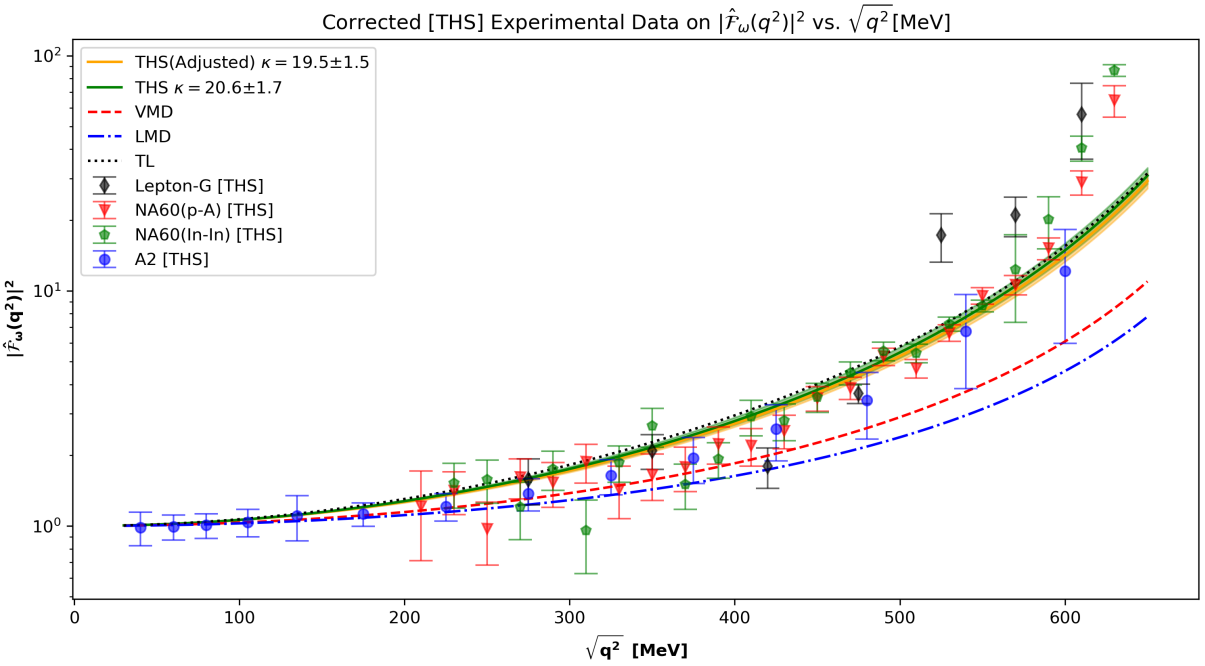

Figure 8: The corrected data using THS with adjusted and non-adjusted κ. The corrected data points from the four separate experiments with the four different form factor models $|\hat{\mathcal{F}}_\omega(q^2)|^2$ are plotted. The data was corrected using THS with $\kappa = 19.5 \pm 1.5$ with both $\kappa = 19.5 \pm 1.5$ and $\kappa = 20.6 \pm 1.7$ plotted as well as their associated error bands.

As the A2 experimental data set showed the most significant correction the continues error bands were plotted in Fig. 6b. The other data sets were not plotted with continuous error bands as again barely any deviation was visibly between the uncorrected and corrected data. All the corrected data are plotted in Fig. 8. These data points were also corrected using the adjusted THS with the other form factor models included as well. Once again the most obvious difference in the data is for the A2 data from the electron channel. The Λ^{-2} parameter for the corrected A2 data set was found to be $\Lambda^{-2}_{\text{A2 Corrected}} = 2.02 \pm 0.02\,\text{GeV}^{-2}$ compared with the fit for the uncorrected A2 data set of $\Lambda^{-2}_{\text{A2}} = 1.99 \pm 0.21\,\text{GeV}^{-2}$ [14] where the greater uncertainty comes from the total uncertainty rather than just the uncertainty from the fit done for the corrected data. For the other data sets the difference between the corrected and uncorrected fit was minimal enough to not be worth further study.

5 Discussion

One of the goals of addressing the NLO calculation of the ω Dalitz decays was to go beyond the soft-photon approximation. This was done by performing the BS integral over the full range of the s_γ values as seen in Appendix C. Eqs. (45), (46), (51) demonstrate that ultimately the IR divergence are cancelled as the only divergent terms left are the $\log m/\Lambda$ terms that will cancel with the $\log m/\Lambda$ term from the virtual corrections. The final expression for the $J[1/AB]$ integral unfortunately could not be integrated further over the variable u introduced with the Feynman parametrization. No analytical solution seems to exist either for the integral at this stage. The total corrections $\delta(x)$ as seen in

Fig. 4 have similar patterns in both channels, starting out positive and then becoming negative as $x \to 1$.The electron channel also shows a larger magnitude correction than the muon channel. This can be seen when comparing the THS corrections in Fig. 6 where the A2 electron data is easier to see the corrections in than the muon data from the other experimental data.

When the form factor data was reevaluated using the radiative corrections, the expectation would have been that including radiative corrections and as well as going beyond the soft-photon approximation could possibly lead to addressing the deviation between experiment and theory. As seen in Fig. 5, neither FF model manages to fully describe the experimental data with the values for large $\sqrt{q^2}$ deviating strongly. When the corrections were then applied, this deviation from the expected value was then hoped to be reduced in magnitude. However, as can be seen in Fig. 4 the correction for the electron and muon channels start out positive and then for large x values (i.e. larger $\sqrt{q^2}$ using $q^2 = x\Delta_M^2$) becomes negative. This means when the correction is applied using Eq. (63) the values for small $\sqrt{q^2}$ (where there was no apparent deviation) are reduced in magnitude, while for the larger $\sqrt{q^2}$ values the magnitude is increased. This means that the magnitude of the deviation is actually reinforced due to the value of the correction for large $\sqrt{q^2}$. Looking at the Λ^{-2} parameters for the A2 data, the corrected fit $\Lambda^{-2}_{\text{A2 Corrected}} = 2.02 \pm 0.02\,\text{GeV}^{-2}$ brings the A2 Λ^{-2} value closer to the fitted values for the NA60(p-A) and NA60(In-In) values, $\Lambda^{-2}_{\text{NA60(p-A)}} = 2.223 \pm 0.026\,\text{GeV}^{-2}$ and $\Lambda^{-2}_{\text{NA60(In-In)}} = 2.24 \pm 0.06\,\text{GeV}^{-2}$ respectively. This suggests that the correction ultimately makes the different data sets converge but the deviation between theory and experiment is not addressed. This result makes it clear that the NLO QED radiative corrections beyond the soft-photon approximations are not enough to address the deviation. These results were calculated for several different form factor models but as seen in Fig. 4, they all show the same kind of general behavior for large and small $\sqrt{q^2}$ values. Thus the corrections are seemingly overall model-independent justifying the choice to focus on using the THS model in computing the corrections. Moreover, the differences between the soft-photon approximation curve and form factor models curves are small, hence the possibility of adding the resonance widths into the form factor expressions can be expected to have a small impact on the corrections. The overall result for the correction indicates that the current theoretical background used for describing form factor models might be missing something when it comes to tackling the electromagnetic form factors involved in the ω Dalitz decays. Whether this is the result of new physics or if there are models consistent with the SM that could explain these results is currently unknown and more research is necessary to explore these options. Using the corrections as seen in Fig. 4, some insights can be gained into which form factor models are feasible for describing the decay. As the correction is more significant for A2 data this is where the most insight can be gained. In the uncorrected data as seen in Fig. 5, the A2 data uncertainty range barely incorporated the LMD and VMD models. With the corrections the LMD model now falls outside bounds of the A2 data points for higher $\sqrt{q^2}$ while the VMD model is included at the lower end of the A2 data. This result is consistent with the other data sets that seemingly are not consistent with the LMD or the VMD models as well.

Possible new avenues of research for addressing this problem include both experimental and theoretical approaches. When it comes to experiments, more data is necessary. The Lepton-G results is based of only 60 events [13] collected in 1981 and the NA60(In-In) heavy-ion experiment collected the ω Dalitz decay data as a side product of studying the heavy-ion collisions and as such was not a targeted search [12]. More experimental data is

vital to ensure that error is minimized and that the observed deviation is not an artifact of uncertainties in the data although this seems not to be the case. More data from the electron channel with minimized uncertainty could shed more light on which models are excluded from the experimental data and thereby reduce the number of suitable theoretical approaches. When it comes to tackling the problem from the theoretical perspective, there are numerous ways to approach. The VMD and LMD models clearly show some incompatibility with data in the higher $\sqrt{q^2}$ region but are consistent with lower energies and extensions of these models in the form of TL and THS models are shown to be more consistent with the data. The most obvious avenue of research would then be to explore whether or not extensions of the TL or THS models can incorporate or at least minimize this deviation to be within experimental error. If no extension is found a new approach needs to be developed that might be more successful for describing this type of decay but significant deviations from the other form factor models could be difficult due to the other models having been successfully implemented in other decays. This opens up the possibility that there might be exotic physics from outside the SM that is affecting the results. What the shape of this type of exotic phenomenon would take is at this point unclear but remains an option worth exploring. More research will inevitably shed insight into the problem which could eventually be addressed within the confines of the SM and exhausting SM approaches remains vital. Whether or not this is the case can only be answered through more experimental data, specifically more precise data to minimize uncertainties.

The results for the radiative corrections for the soft-photon approximation and the result for going beyond the soft-photon approximation can also be compared. The soft-photon approximation remains larger in magnitude than the full radiative corrections in both the electron and muon channel. For both channels, the soft-photon approximation actually remains positive over a larger range of x values compared with the full corrections as seen in Fig. 4. This means that the new estimates for the form factor data is pushed towards smaller values when using the soft-photon approximation. We can also compare the soft-photon bremsstrahlung and the full corrections. In the muon channel, the full corrections would now instead push the estimates towards smaller values compared with the soft-photon bremsstrahlung. In the electron channel, the soft-photon bremsstrahlung misses the entire positive region for the correction. This means that, ultimately, the soft-photon bremsstrahlung, soft-photon approximation, and full corrections all reinforce the deviation. Going beyond the soft-photon approximation can therefore not address this deviation between theory and experiment.

When using the radiative corrections, there are different times when either the full radiative corrections or the soft-photon bremsstrahlung would be appropriate. In an experiment where the final-state photon from the BS could be detected, this will have a certain resolution below which photons of a certain energy cannot be detected. Using the cutoff with the soft-photon bremsstrahlung would then capture the radiative corrections below that resolution. The result for going beyond the soft-photon approximation would then be appropriate for the case of where the BS photon is not detected or ignored in the experiment and as such needs to include the full range of possible photon values. As a result, the radiative corrections need to be tailored to the specific experimental set-up being considered.

6 Conclusion

Introducing the NLO QED radiative corrections and taking into account hard photons for the BS phenomenon did not resolve the deviation between the theoretical form factor models and the experimental data on the $\omega \to \pi^0 \ell^+ \ell^-$ decays. The extent of the deviation was in fact increased suggesting a more significant readjustment of the approach to form factor models for the $\omega \to \pi\gamma$ transition. The results for the correction did demonstrate the apparent incompatibility for the LMD model with any of the sets of data. Finally the result demonstrates the need for more data on these ω decays and the need for further investigation of new possible ways to extend the form factor models or as a last resort to consider new physics contributing.

A List of Integrals

Full list of basic integrals related to the IR-convergent part of the matrix element squared. This mostly a repeat of similar results from Ref. [6].
The following function is defined for simplicity

$$L(a,b,c) = \frac{1}{\sqrt{a^2-b}} \log\left|\frac{c+a+\sqrt{a^2-b}}{c+a-\sqrt{a^2-b}}\right|. \tag{A.1}$$

In the reference frame $\mathbf{p}_1 - \mathbf{q}_1 - \mathbf{q}_2 = 0$ the energies of the leptons can be written as:

$$\omega q_{1,0} = (k+p_2)\cdot q_1 = \frac{1}{4}(m_\omega^2 - s - s_\gamma - \Delta_m^2)\,, \tag{A.2}$$

$$\omega q_{2,0} = (k+p_2)\cdot q_2 = \frac{1}{4}(m_\omega^2 - s - s_\gamma + \Delta_m^2)\,. \tag{A.3}$$

The integrals can then be written as

$$J[1] = \frac{\tilde{\omega}}{\omega}\,, \tag{A.4}$$

$$J[A] = \frac{\tilde{\omega}^2}{\omega^2}\frac{\omega q_{2,0}}{2}\,, \tag{A.5}$$

$$J\left[\frac{1}{A}\right] = L(\omega q_{2,0}, \omega^2 m^2, 0)\,, \tag{A.6}$$

$$J\left[\frac{1}{E}\right] = \frac{1}{2}L(\omega(q_{1,0}+q_{2,0}), \omega^2 s, \frac{\omega}{\tilde{\omega}}\tilde{s})\,, \tag{A.7}$$

$$J\left[\frac{1}{AB}\right] = \frac{8}{\tilde{\omega}\omega}L(s, 4m^2 s, 0)\,, \tag{A.8}$$

$$J\left[\frac{1}{A^2}\right] = \frac{4}{m^2\tilde{\omega}\omega}\,, \tag{A.9}$$

$$J\left[\frac{1}{E^2}\right] = \frac{1}{s}\frac{\tilde{\omega}\omega}{\tilde{\omega}\omega(M_\omega^2 - m_\pi^2) + s m_\pi^2}\,. \tag{A.10}$$

For the other integrals the following variables are useful as well

$$v_1 = \omega q_{2,0}\frac{\tilde{\omega}}{\omega}\,, \tag{A.11}$$

$$v_2 = \omega q_{1,0}\frac{\tilde{\omega}}{\omega} + \tilde{s}\,, \tag{A.12}$$

$$w_0 = m^2\tilde{\omega}^2\,, \tag{A.13}$$

$$w_1 = (s-2m^2)\tilde{\omega}^2 + 2\tilde{s}\omega q_{2,0}\frac{\tilde{\omega}}{\omega}\,, \tag{A.14}$$

$$w_2 = m^2\tilde{\omega}^2 + \tilde{s}^2 + 2\tilde{s}\omega q_{1,0}\frac{\tilde{\omega}}{\omega}\,, \tag{A.15}$$

$$\varrho = 2w_0 + w_1\,, \tag{A.16}$$

$$\tilde{\varrho} = 2w_2 + w_1\,, \tag{A.17}$$

$$\zeta = w_1^2 - 4w_0 w_2\,, \tag{A.18}$$

$$w = w_0 + w_1 + w_2\,, \tag{A.19}$$

$$\tau_1 = v_2\varrho - v_1\tilde{\varrho}\,, \tag{A.20}$$

$$\tau_2 = v_1 w_1 - 2v_2 w_0\,, \tag{A.21}$$

$$\tau = v_1^2 w_2 + v_2^2 w_0\,. \tag{A.22}$$

The rest of the integrals then become

$$J\left[\frac{1}{AE}\right] = \frac{2\tilde{\omega}}{\omega}\frac{1}{\sqrt{\zeta}}\log\left[\frac{\varrho+\sqrt{\zeta}}{\varrho-\sqrt{\zeta}}\right], \tag{A.23}$$

$$J\left[\frac{1}{AE^2}\right] = \frac{2}{\zeta}\left\{\tau_1\frac{2\tilde{\omega}}{\omega}\frac{1}{w} + \tau_2 J\left[\frac{1}{AE}\right]\right\}, \tag{A.24}$$

$$J\left[\frac{1}{A^2E}\right] = \frac{4}{\zeta}\left\{\tau_2\frac{2\tilde{\omega}}{\omega}\frac{1}{w_0} + \tau_1 J\left[\frac{1}{AE}\right]\right\}, \tag{A.25}$$

$$\begin{aligned} J\left[\frac{1}{A^2E^2}\right] = \frac{16}{\zeta}\Bigg\{&\frac{2\tilde{\omega}}{\omega}\left[\frac{1}{2}\left(1 + \frac{v_1^2}{w_0} + \frac{(v_1+v_2)^2}{w}\right) + \frac{6}{\zeta}(\tau - v_1 v_2 w_1)\right] \\ &- \left[\frac{\varrho}{4} - 2v_1v_2 + v_1^2 + \frac{3}{\zeta}(\tau\varrho - 2v_1v_2w_0\tilde{\varrho})\right] J\left[\frac{1}{AE}\right]\Bigg\}. \end{aligned} \tag{A.26}$$

Other integrals of the form

$$J\left[\frac{1}{X(E-M_V^2)}\right] = J\left[\frac{1}{XE}\right]_{\tilde{s}\to s-M_V^2}\,, \tag{A.27}$$

where $X \in \{1, A, A^2\}$. Here $\tilde{s} \to s - M_V^2$ indicates that in previous expressions where $\tilde{s}$ appears it is replaced by $s - M_V^2$ to get the integrals. For similar integrals of the form

$$J\left[\frac{1}{Y(E-M_V^2)^2}\right] = J\left[\frac{1}{YE^2}\right]_{\tilde{s}\to s-M_V^2}\,, \tag{A.28}$$

for $Y \in \{A, A^2\}$. For the final term for $Y = 1$ we find

$$J\left[\frac{1}{(E-M_V^2)^2}\right] = \frac{\omega\tilde{\omega}}{\omega^2\tilde{s}^2 + \tilde{\omega}^2\omega^2 s + \tilde{s}\tilde{\omega}\omega(m_\omega^2 - s - s_\gamma)}\,. \tag{A.29}$$

The terms $J\left[\frac{1}{A^2E}\right]$, $J\left[\frac{1}{A^2(E-M_V^2)}\right]$, $J\left[\frac{1}{A^2E^2}\right]$, and $J\left[\frac{1}{A^2(E-M_V^2)^2}\right]$ all contain the divergent parts $\frac{1}{s}J\left[\frac{1}{A^2}\right]$, $\frac{1}{s-M_V^2}J\left[\frac{1}{A^2}\right]$, $\frac{1}{s^2}J\left[\frac{1}{A^2}\right]$ and $\frac{1}{(s-M_V^2)^2}J\left[\frac{1}{A^2}\right]$ respectively that have to be dealt with before being numerically integrated over. Rewriting the integrals to remove the divergences then yields:

$$J\left[\frac{1}{A^2E}\right]\Big|_{\text{Conv.}} = \left(\frac{2\tau_2}{\zeta} - \frac{1}{s}\right)\frac{4}{m^2\omega\tilde{\omega}} + \frac{4}{\zeta}\left\{\tau_1 J\left[\frac{1}{AE}\right]\right\}, \tag{A.30}$$

$$J\left[\frac{1}{A^2(E-M_V^2)}\right]\Big|_{\text{Conv.}} = (\frac{2\tau_1}{\zeta} - \frac{1}{s-M_V^2})\frac{4}{m^2\omega\tilde{\omega}} + \frac{2}{\zeta}\left\{\tau_2 J\left[\frac{1}{AE}\right]\right\}. \tag{A.31}$$

and

$$\begin{aligned} J\left[\frac{1}{A^2E^2}\right]\Big|_{\text{Conv.}} = &\left(\frac{4v_1^2}{\zeta} - \frac{1}{s^2}\right)\frac{4}{m^2\tilde{\omega}\omega} \\ &+ \frac{16}{\zeta}\Big\{\frac{2\tilde{\omega}}{\omega}\left[\frac{1}{2}\left(1 + \frac{(v_1+v_2)^2}{w}\right) + \frac{6}{\zeta}(\tau - v_1v_2w_1)\right] \\ &- \left[\frac{\varrho}{4} - 2v_1v_2 + v_1^2 + \frac{3}{\zeta}(\tau\varrho - 2v_1v_2w_0\tilde{\varrho})\right] J\left[\frac{1}{AE}\right]\Big\}. \end{aligned} \tag{A.32}$$

and finally

$$\begin{aligned} J\left[\frac{1}{A^2(E-M_V^2)^2}\right]\Big|_{\text{Conv.}} = &\left(\frac{4v_1^2}{\zeta} - \frac{1}{(s-M_V^2)^2}\right)\frac{4}{m^2\tilde{\omega}\omega} \\ &+ \frac{16}{\zeta}\Big\{\frac{2\tilde{\omega}}{\omega}\left[\frac{1}{2}\left(1 + \frac{(v_1+v_2)^2}{w}\right) + \frac{6}{\zeta}(\tau - v_1v_2w_1)\right] \\ &- \left[\frac{\varrho}{4} - 2v_1v_2 + v_1^2 + \frac{3}{\zeta}(\tau\varrho - 2v_1v_2w_0\tilde{\varrho})\right] J\left[\frac{1}{AE}\right]\Big\}. \end{aligned} \tag{A.33}$$

For the final integrals left it is convenient to define

$$b_i = \frac{q_{i,0}}{|\mathbf{q}_i|}\,, \tag{A.34}$$

$$|\mathbf{q}_i| = \sqrt{q_{i,0}^2 - m^2}\,, \tag{A.35}$$

$$\eta = \frac{\mathbf{q}_1\cdot\mathbf{q}_2}{|\mathbf{q}_1||\mathbf{q}_2|} = b_1b_2 - \frac{1}{2}\frac{(s-2m^2)}{|\mathbf{q}_1||\mathbf{q}_2|}\,. \tag{A.36}$$

Another set of functions can be defined:

$$\tilde{Q}_1(\xi) \equiv b_1 Q_0(\xi) - \eta Q_1(\xi)\,, \tag{A.37}$$

$$\tilde{Q}_2(\xi) \equiv \left(\frac{1}{3} + b_1^2\right) Q_0(\xi) - 2b_1\eta Q_1(\xi) + \left(\eta^2 - \frac{1}{3}\right) Q_2(\xi)\,. \tag{A.38}$$

Here $Q_m(\xi)$ are the Legendre functions of second kind and we have introduced a redefinition for $Q_0(\xi)$ for $\xi > 1$ such that

$$Q_0(\xi) = \frac{1}{2}\log\left(\frac{\xi+1}{\xi-1}\right), \tag{A.39}$$

$$Q_1(\xi) = \xi Q_0(\xi) - 1\,, \tag{A.40}$$

$$Q_2(\xi) = \frac{1}{2}(3\xi^2 - 1)Q_0(\xi) - \frac{3}{2}\xi\,. \tag{A.41}$$

The final mixed integrals then give

$$J\left[\frac{B}{A}\right] = \frac{\tilde{\omega}}{\omega}\frac{|\mathbf{q}_1|}{|\mathbf{q}_2|}\tilde{Q}_1(b_2)\,, \tag{A.42}$$

$$J\left[\frac{B}{A^2}\right] = -\frac{2}{\omega}\frac{|\mathbf{q}_1|}{|\mathbf{q}_2|^2}\frac{d\tilde{Q}_1(\xi)}{d\xi}\Big|_{\xi=b_2}, \tag{A.43}$$

$$J\left[\frac{B^2}{A}\right] = \frac{\tilde{\omega}^2}{2\omega}\frac{|\mathbf{q}_1|^2}{|\mathbf{q}_2|}\tilde{Q}_2(b_2)\,, \tag{A.44}$$

$$J\left[\frac{B^2}{A^2}\right] = -\frac{\tilde{\omega}}{\omega}\frac{|\mathbf{q}_1|^2}{|\mathbf{q}_2|^2}\frac{d\tilde{Q}_2(\xi)}{d\xi}\Big|_{\xi=b_2}. \tag{A.45}$$

B Derivation of IR-divergent Expression

We can write

$$J[f(k,p_2)] = \frac{1}{2\pi}\int \frac{\mathrm{d}^3\boldsymbol{k}}{k_0}\frac{\mathrm{d}^3\boldsymbol{p}_2}{p_{20}} f(k,p_2)\delta^4(p_1 - q_1 - q_2 - k - p_2)\,.$$

We want to get an expression for IR-divergent expressions. So we can start with $\frac{1}{AB}$ and define that:

$$A = k\cdot q_2\,,$$
$$B = k\cdot q_1\,,$$

where q_2 is the positron four-momentum and q_1 is the electron four-momentum. Using Feynman parametrization we can then rewrite $\frac{1}{AB}$

$$\frac{1}{AB} = \int_0^1 \frac{1}{[uA + (1-u)B]^2}\,\mathrm{d}u\,.$$

So rewriting using k for the photon four-momentum

$$\frac{1}{AB} = \int_0^1 \frac{1}{(k\cdot[uq_2 + (1-u)q_1])^2}\,\mathrm{d}u\,.$$

We now use the delta function to integrate away $d^3\boldsymbol{p}_2$ so that we have

$$J[\frac{1}{AB}] = \frac{1}{2\pi}\int \frac{\mathrm{d}^3\boldsymbol{k}}{k_0 p_{20}}\frac{1}{AB}\delta(p_{10} - q_{10} - q_{20} - k_0 - p_{20})\,.$$

Rewriting $\mathrm{d}^3\boldsymbol{k} = \mathrm{d}|\boldsymbol{k}| \cdot |\boldsymbol{k}|^2 \mathrm{d}\Omega$ we then have

$$J[\frac{1}{AB}] = \int \frac{\mathrm{d}|\boldsymbol{k}| \cdot |\boldsymbol{k}|^2 \mathrm{d}(\cos\theta_{\boldsymbol{k}})}{k_0 p_{20}} \frac{1}{AB} \delta(p_{10} - q_{10} - q_{20} - k_0 - p_{20}) \,.$$

Now we can define

$$\begin{aligned} A_1 &= [uq_{20} + (1-u)q_{10}] \,, \\ A_2 &= |u\boldsymbol{q_2} + (1-u)\boldsymbol{q_1}| \,. \end{aligned}$$

and defining $\mathrm{d}z = \mathrm{d}(\cos\theta_{\boldsymbol{k}})$ we can write

$$\frac{1}{AB} = \int_0^1 \frac{1}{[k_0 \cdot A_1 - |\boldsymbol{k}| A_2 z]^2} \mathrm{d}u \,.$$

So integrating over z

$$\begin{aligned} \int_{-1}^1 \frac{1}{AB} \mathrm{d}z &= \int_0^1 \int_{-1}^1 \frac{1}{[k_0 \cdot A_1 - |\boldsymbol{k}| A_2 z]^2} \mathrm{d}z \mathrm{d}u \\ &= \int_0^1 \frac{2}{k_0^2 A_1^2 - |\boldsymbol{k}|^2 A_2^2} \, \mathrm{d}u \,. \end{aligned}$$

So total expression is then

$$J[\frac{1}{AB}] = \int_0^1 \int \frac{\mathrm{d}|\boldsymbol{k}| \cdot |\boldsymbol{k}|^2}{k_0 p_{20}} \frac{2}{k_0^2 A_1^2 - |\boldsymbol{k}|^2 A_2^2} \delta(p_{10} - q_{10} - q_{20} - k_0 - p_{20}) \mathrm{d}u \,.$$

We have that the mass of the photon (Λ) is non-zero so s_γ then becomes

$$s_\gamma = \Lambda^2 + m_\pi^2 + 2(k_0 p_{20} - \boldsymbol{k} \cdot \boldsymbol{p}_2) \,.$$

Using that $\boldsymbol{p}_2 = -\boldsymbol{k}$ we can then write

$$s_\gamma = \Lambda^2 + m_\pi^2 + 2(k_0 p_{20} + |\boldsymbol{k}|^2) \,.$$

Have that $k_0^2 = \Lambda^2 + |\boldsymbol{k}|^2$ so rewriting this have

$$s_\gamma = m_\pi^2 - \Lambda^2 + 2k_0\sqrt{s_\gamma} \,.$$

So solving for k_0

$$\begin{aligned} 2k_0\sqrt{s_\gamma} &= s_\gamma - m_\pi^2 + \Lambda^2 \\ &\leftrightarrow \\ k_0 &= \frac{s_\gamma - m_\pi^2 + \Lambda^2}{2\sqrt{s_\gamma}} \,. \end{aligned}$$

Using this we can solve for $k_0 p_{20}$

$$k_0 p_{20} = \frac{s_\gamma^2 - (m_\pi^2 - \Lambda^2)^2}{4 s_\gamma} \,.$$

So then combining this to solve for $|\boldsymbol{k}|^2$

$$|\boldsymbol{k}|^2 = \frac{(s_\gamma - (m_\pi^2 + \Lambda^2))^2 - 4m_\pi^2\Lambda^2}{4s_\gamma}\,.$$

Now we want to introduce a change in variables in the integrals such that $a = \sqrt{s_\gamma}$. So we need to evaluate $\frac{\mathrm{d}|\boldsymbol{k}|}{\mathrm{d}a}$

$$\frac{\mathrm{d}|\boldsymbol{k}|}{\mathrm{d}a} = \frac{s_\gamma^2 - (m_\pi^2 - \Lambda^2)^2}{2s_\gamma\sqrt{(s_\gamma - (m_\pi^2 + \Lambda^2))^2 - 4m_\pi^2\Lambda^2}}\,.$$

So then using these results can write

$$J[\frac{1}{AB}] = \int_0^1 \int \mathrm{d}\sqrt{s_\gamma}\frac{\sqrt{(s_\gamma - (m_\pi^2 + \Lambda^2))^2 - 4m_\pi^2\Lambda^2}}{2s_\gamma}\frac{2}{k_0^2A_1^2 - |\boldsymbol{k}|^2A_2^2}$$
$$\delta(p_{10} - q_{10} - q_{20} - k_0 - p_{20})\mathrm{d}u\,.$$

Then rewriting the delta function using $p - k - q_1 - q_2 - p_2 = 0$ and $\boldsymbol{p}_2 = -\boldsymbol{k}$ we get

$$\delta(\sqrt{s_\gamma} - (p_{10} - q_{10} - q_{20}))\,.$$

Then we simply have

$$J[\frac{1}{AB}] = \int_0^1 \frac{\sqrt{(s_\gamma - (m_\pi^2 + \Lambda^2))^2 - 4m_\pi^2\Lambda^2}}{2s_\gamma}\frac{2}{k_0^2A_1^2 - |\boldsymbol{k}|^2A_2^2}\,\mathrm{d}u\,.$$

Now we need to look at the $\frac{2}{k_0^2A_1^2 - |\boldsymbol{k}|^2A_2^2}$ term

$$\frac{2}{k_0^2A_1^2 - |\boldsymbol{k}|^2A_2^2} = \frac{8s_\gamma}{(s_\gamma - (m_\pi^2 + \Lambda^2))^2 - 4m_\pi^2\Lambda^2)(A_1^2 - A_2^2) + 4s_\gamma\Lambda^2A_1^2}\,.$$

So then we have

$$J[\frac{1}{AB}] = 4\int_0^1 \frac{\sqrt{(s_\gamma - (m_\pi^2 + \Lambda^2))^2 - 4m_\pi^2\Lambda^2}}{(s_\gamma - (m_\pi^2 + \Lambda^2))^2 - 4m_\pi^2\Lambda^2)(A_1^2 - A_2^2) + 4s_\gamma\Lambda^2A_1^2}\,\mathrm{d}u\,.$$

Now we need to deal with $4s_\gamma\Lambda^2A_1^2$ so that we can write

$$4s_\gamma\Lambda^2A_1^2 = \frac{1}{4}[m_\omega^2 - s - s_\gamma + (2u-1)\Delta_m^2]^2\,.$$

Finally looking at $A_1^2 - A_2^2$ we find that we can write it as

$$A_1^2 - A_2^2 = m^2 + u(1-u)(s - 4m^2)\,.$$

So the total final expression is then:

$$4\int_0^1 \int_{s_\gamma^{\min}}^{s_\gamma^{\max}} \frac{\sqrt{\lambda(s_\gamma, m_\pi^2, \Lambda^2)}}{\lambda(s_\gamma, m_\pi^2, \Lambda^2)(A_1^2 - A_2^2) + 4s_\gamma\Lambda^2A_1^2}\,\mathrm{d}s_\gamma\mathrm{d}u\,.$$

C Partial Integral of the IR-divergent Expression

From the final expression of the divergent expression we have that $J\left[1/AB\right]$ can be written as

$$J\left[\frac{1}{AB}\right] = 4\int_0^1 \int_{s_\gamma^{\min}}^{s_\gamma^{\max}} \frac{\sqrt{\lambda(s_\gamma, m_\pi^2, \Lambda^2)}}{\lambda(s_\gamma, m_\pi^2, \Lambda^2)(A_1^2 - A_2^2) + 4s_\gamma \Lambda^2 A_1^2}\, \mathrm{d}s_\gamma \mathrm{d}u\,. \tag{C.1}$$

This integral over s_γ now needs to be evaluated

$$4\int_0^1 \int_{s_\gamma^{\min}}^{s_\gamma^{\max}} \frac{\sqrt{\lambda(s_\gamma, m_\pi^2, \Lambda^2)}}{\lambda(s_\gamma, m_\pi^2, \Lambda^2)(A_1^2 - A_2^2) + 4s_\gamma \Lambda^2 A_1^2}\, \mathrm{d}s_\gamma \mathrm{d}u\,. \tag{C.2}$$

For now we ignore the integral over u. This integral can then be simplified by considering what happens when the Λ is taken to the limit

$$\lim_{\Lambda\to 0} \frac{\sqrt{\lambda(s_\gamma, m_\pi^2, \Lambda^2)}}{\lambda(s_\gamma, m_\pi^2, \Lambda^2)(A_1^2 - A_2^2) + 4s_\gamma \Lambda^2 A_1^2}\, \mathrm{d}s_\gamma \mathrm{d}u\,. \tag{C.3}$$

When this limit is considered, the integral turns out to be able to be simplified to

$$4\int_{s_\gamma^{\min}}^{s_\gamma^{\max}} \frac{\sqrt{\lambda(s_\gamma, m_\pi^2, \Lambda^2)}\mathrm{d}s_\gamma}{\lambda(s_\gamma, m_\pi^2, \Lambda^2)(A_1^2 - A_2^2) + \frac{1}{4}\Lambda^2[m_\omega^2 - s + (2u-1)\Delta_m^2]^2}\,. \tag{C.4}$$

with the two integrals converging in the limit $\Lambda \to 0$. The substitution $a = s_\gamma - (m_\pi^2 + \Lambda^2)$ with $da/ds_\gamma = 1$, $F^2 = 4m_\pi^2\Lambda^2$, $V = (m^2 + u(1-u)(s-4m^2)$, and $B = \frac{1}{4}\Lambda^2[m_\omega^2 - s + (2u-1)\Delta_m^2]^2$ such that

$$4\int_{a^{\min}}^{a^{\max}} \frac{\sqrt{a^2 - F^2}\,\mathrm{d}a}{(a^2 - F^2)V + B}\,. \tag{C.5}$$

Here a trig substitution is performed with $a = F\sec j$. This has $\frac{\mathrm{d}a}{\mathrm{d}j} = F\sec j\tan j$. Using this we can rewrite the integral as

$$4\int_{j^{\min}}^{j^{\max}} \frac{F^2\sec j\tan^2 j\,\mathrm{d}j}{F^2\tan^2 jV + B}\,. \tag{C.6}$$

Rewriting in terms of $\cos j$ and $\sin j$ we get

$$4\int_{j^{\min}}^{j^{\max}} \frac{F^2\sin^2 j\,\mathrm{d}j}{F^2\sin^2 j\cos jV + B\cos^3 j}\,. \tag{C.7}$$

Multiplying by $\frac{\cos j}{\cos j}$ we can further rewrite

$$4\int_{j^{\min}}^{j^{\max}} \frac{F^2\sin^2 j\cos j\,\mathrm{d}j}{\cos^2 j(F^2V\sin^2 j + B\cos^2 j)}\,. \tag{C.8}$$

This can further be written as

$$4\int_{j^{\min}}^{j^{\max}} \frac{-F^2\sin^2 j\cos j\,\mathrm{d}j}{(\sin j - 1)(\sin j + 1)((F^2V - B)\sin^2 j + B)}\,. \tag{C.9}$$

Now we introduce a new variable $W = \sin j$ with $\frac{\mathrm{d}W}{\mathrm{d}j} = \cos j$ which allows one to write $\mathrm{d}j = \frac{\mathrm{d}W}{\cos j}$ so that we can write

$$4\int_{W^{\min}}^{W^{\max}} \frac{-F^2W^2}{(W-1)(W+1)((F^2V-B)W^2+B)}\mathrm{d}W\,. \tag{C.10}$$

Performing partial decomposition this gives

$$-4F^2\int_{W^{\min}}^{W^{\max}} \frac{B}{F^2V(F^2V-B)W^2+B} - \frac{1}{2F^2V(W+1)} + \frac{1}{2F^2V(W+1)}\mathrm{d}W\,. \tag{C.11}$$

Looking at the first part of this expression we introduce a new variable $y = \frac{\sqrt{F^2V-B}W}{\sqrt{B}}$ with $\mathrm{d}W = \frac{\sqrt{B}}{\sqrt{F^2V-B}}\mathrm{d}y$ so the integral then becomes

$$-\frac{4}{V}\int_{y^{\min}}^{y^{\max}} \frac{\sqrt{B}\mathrm{d}y}{\sqrt{F^2V-B}(y^2+1)}\,. \tag{C.12}$$

Which is then simply

$$-\frac{4\sqrt{B}}{V\sqrt{F^2V-B}}\int_{y^{\min}}^{y^{\max}} \frac{\mathrm{d}y}{(y^2+1)}\,. \tag{C.13}$$

Which is just the integral for the arctan so this becomes

$$-\frac{4\sqrt{B}}{V\sqrt{F^2V-B}}\left[\arctan y\right]_{y_{\min}}^{y_{\max}}\,. \tag{C.14}$$

In terms of W this becomes

$$-\frac{4\sqrt{B}}{V\sqrt{F^2V-B}}\left[\arctan\frac{\sqrt{F^2V-B}W}{\sqrt{B}}\right]_{W_{\min}}^{W_{\max}}\,. \tag{C.15}$$

Looking at the other integrals these are simply logarithms so the entire expression yields

$$\left[-\frac{4\sqrt{B}}{V\sqrt{F^2V-B}}\arctan\frac{\sqrt{F^2V-B}W}{\sqrt{B}} - \frac{2}{V}\log|W-1| + \frac{2}{V}\log|W+1|\right]_{W^{\min}}^{W^{\max}}\,. \tag{C.16}$$

The logarithms can then be combined to one expression

$$\frac{2}{V}\log\left|\frac{W+1}{W-1}\right|. \tag{C.17}$$

Using the definition of W we can write

$$W = \sin j = \sin\left(arcsec(\frac{a}{F})\right) = \frac{\sqrt{a^2-F^2}}{a}. \tag{C.18}$$

So the logarithm then becomes

$$\frac{2}{V}\log\left|\frac{\sqrt{a^2-F^2}+a}{\sqrt{a^2-F^2}-a}\right|. \tag{C.19}$$

Rewriting this have

$$\frac{2}{V}\log\Big|\frac{a+\sqrt{a^2-F^2}}{a-\sqrt{a^2-F^2}}\Big|. \tag{C.20}$$

Doing this for arctan have

$$-\frac{4\sqrt{B}}{V\sqrt{F^2V-B}}\arctan\Big(\frac{\sqrt{F^2V-B}}{\sqrt{B}}\frac{\sqrt{a^2-F^2}}{a}\Big). \tag{C.21}$$

Now can rewrite the logarithm further

$$\frac{2}{V}\log\Big|\frac{a+\sqrt{a^2-F^2}}{a-\sqrt{a^2-F^2}}\frac{a+\sqrt{a^2-F^2}}{a+\sqrt{a^2-F^2}}\Big| = \frac{2}{V}\log\Big|\frac{(a+\sqrt{a^2-F^2})^2}{F^2}\Big|. \tag{C.22}$$

This can further be rewritten using the definition of F^2 as

$$\frac{2}{V}\log\Big|\frac{(a+\sqrt{a^2-F^2})^2}{4m_\pi^2\Lambda^2}\frac{m^2}{m^2}\Big| = \frac{4}{V}\log\Big|\frac{(a+\sqrt{a^2-F^2})}{2m_\pi m}\Big| + \frac{4}{V}\log\Big|\frac{m}{\Lambda}\Big|. \tag{C.23}$$

Using the definition of a and F^2 we can then write

$$\frac{4}{V}\log\Big|\frac{(s_\gamma-(m_\pi^2+\Lambda^2)+\sqrt{(s_\gamma-(m_\pi^2+\Lambda^2))^2-4m_\pi^2\Lambda^2})}{2m_\pi m}\Big| + \frac{4}{V}\log\Big|\frac{m}{\Lambda}\Big|. \tag{C.24}$$

Now can consider what happens when taking the integration limits on this logarithm. For $s_\gamma^{\min}=(m_\pi+\Lambda)^2$ the logarithm can be written as

$$\frac{4}{V}\log\Big|\frac{((m_\pi+\Lambda)^2-(m_\pi^2+\Lambda^2))}{2m_\pi m}\Big| + \frac{4}{V}\log\Big|\frac{m}{\Lambda}\Big| \tag{C.25}$$

$$= \frac{4}{V}\log\Big|\frac{2m_\pi\Lambda}{2m_\pi m}\Big| + \frac{4}{V}\log\Big|\frac{m}{\Lambda}\Big| = 0\,. \tag{C.26}$$

So the total integral for the logarithm is then simply

$$\frac{4}{V}\log\Big|\frac{(s_\gamma^{\max}-(m_\pi^2+\Lambda^2)+\sqrt{(s_\gamma^{\max}-(m_\pi^2+\Lambda^2))^2-4m_\pi^2\Lambda^2})}{2m_\pi m}\Big| + \frac{4}{V}\log\Big|\frac{m}{\Lambda}\Big|. \tag{C.27}$$

Now we can consider taking the limit $\Lambda\to 0$ and dropping the absolute value on the $\log m/\Lambda$ logarithm as it will always be positive, the first logarithm becomes

$$\frac{4}{V}\log\Big|\frac{s_\gamma^{\max}-m_\pi^2}{m_\pi m}\Big| + \frac{4}{V}\log\frac{m}{\Lambda}\,. \tag{C.28}$$

Now we need to consider the arctan. Using the definition of a we can write

$$-\frac{4\sqrt{B}}{V\sqrt{F^2V-B}}\arctan\Big(\frac{\sqrt{F^2V-B}}{\sqrt{B}}\frac{\sqrt{(s_\gamma-(m_\pi^2+\Lambda^2))^2-F^2}}{s_\gamma-(m_\pi^2+\Lambda^2)}\Big). \tag{C.29}$$

For $s_\gamma^{\min}$, the term $\sqrt{(s_\gamma^{\min}-(m_\pi^2+\Lambda^2))^2-F^2}$ is just zero and since $\arctan 0=0$ the total arctan expression over the integration limits is

$$-\frac{4\sqrt{B}}{V\sqrt{F^2V-B}}\arctan\Big(\frac{\sqrt{F^2V-B}}{\sqrt{B}}\frac{\sqrt{(s_\gamma^{\max}-(m_\pi^2+\Lambda^2))^2-F^2}}{s_\gamma^{\max}-(m_\pi^2+\Lambda^2)}\Big). \tag{C.30}$$

Now the limit $\Lambda \to 0$ needs to be considered. Looking at the ratio $\sqrt{(s_\gamma^{\max} - (m_\pi^2 + \Lambda^2))^2 - F^2}/(s_\gamma^{\max} - (m_\pi^2 + \Lambda^2))$ we find

$$\lim_{\Lambda \to 0} \frac{\sqrt{(s_\gamma^{\max} - (m_\pi^2 + \Lambda^2))^2 - F^2}}{s_\gamma^{\max} - (m_\pi^2 + \Lambda^2)} = 1\,.$$

Now we consider the other ratio $\frac{\sqrt{F^2V - B}}{\sqrt{B}}$ in the limit:

$$\lim_{\Lambda \to 0} \frac{\sqrt{F^2V - B}}{\sqrt{B}} = \frac{\sqrt{4m_\pi^2 V - \frac{1}{4}[m_\omega^2 - s + (2u-1)\Delta_m^2]^2}}{\sqrt{\frac{1}{4}[m_\omega^2 - s + (2u-1)\Delta_m^2]^2}}\,.$$

Now we can introduce a new variable Q defined as

$$Q = \frac{1}{4}[m_\omega^2 - s + (2u-1)\Delta_m^2]^2\,. \tag{C.31}$$

So then we can rewrite the expression as

$$\frac{\sqrt{4m_\pi^2 V - Q}}{\sqrt{Q}} = \sqrt{\frac{16m_\pi^2 V}{4Q} - 1}\,. \tag{C.32}$$

This allows for writing the arctan as

$$-\frac{4}{V}\frac{1}{\sqrt{\frac{16m_\pi^2 V}{4Q} - 1}} \arctan\Big(\sqrt{\frac{16m_\pi^2 V}{4Q} - 1}\Big). \tag{C.33}$$

This can be rewritten using $i \operatorname{atanh} z = \arctan iz$ to yield

$$-\frac{4}{V}\frac{1}{\sqrt{1 - \frac{16m_\pi^2 V}{4Q}}} \operatorname{atanh}\Big(\sqrt{1 - \frac{16m_\pi^2 V}{4Q}}\Big). \tag{C.34}$$

Introducing another variable H defined as

$$H = \sqrt{\frac{16m_\pi^2 V}{4Q} - 1}\,. \tag{C.35}$$

The final expression for the total integral becomes

$$\int_0^1 \frac{4}{V}\Big(\log\Big|\frac{s_\gamma^{\max} - m_\pi^2}{m_\pi m}\Big| + \log\frac{m}{\Lambda}\Big) - \frac{4}{V}\frac{1}{H}\operatorname{atanh} H \;\mathrm{d}u\,. \tag{C.36}$$

Now this integral over u can be performed over $\frac{4}{V}$ with the logarithm but the second term cannot be integrated over analytically. Looking at the integral have

$$\int_0^1 \frac{4}{V}\mathrm{d}u = \int_0^1 \frac{4}{(m^2 + u(1-u)(s - 4m^2))}\,\mathrm{d}u\,. \tag{C.37}$$

Using $\beta = \sqrt{1 - \frac{4m^2}{s}}$ this can be rewritten

$$\int_0^1 \frac{4}{(m^2 + u(1-u)(s-4m^2))} \mathrm{d}u = -\frac{4}{s\beta^2} \int_0^1 \frac{1}{-\frac{m^2}{s\beta^2} - u + u^2} \, \mathrm{d}u \,. \tag{C.38}$$

Factoring this expression can write

$$-\frac{4}{s\beta^2} \int_0^1 \frac{1}{(-\frac{m^2}{s\beta^2} - u + u^2} \, \mathrm{d}u = -\frac{4}{s\beta^2} \int_0^1 \frac{1}{(u-u_1)(u-u_2)} \, \mathrm{d}u \,. \tag{C.39}$$

where:

$$u_1 u_2 = -\frac{m^2}{s\beta^2} \,. \tag{C.40}$$

$$u_1 + u_2 = 1 \,. \tag{C.41}$$

Performing partial decomposition this gives

$$-\frac{4}{s\beta^2} \int_0^1 \frac{1}{(u-u_1)(u-u_2)} \mathrm{d}u = -\frac{4}{s\beta^2} \frac{1}{u_2 - u_1} \int_0^1 \frac{1}{u-u_2} - \frac{1}{u-u_1} \, \mathrm{d}u \,. \tag{C.42}$$

This integral is simply

$$\begin{aligned} &- \frac{4}{s\beta^2} \frac{1}{u_2 - u_1} \int_0^1 \frac{1}{u-u_2} - \frac{1}{u-u_1} \mathrm{d}u \\ &= -\frac{4}{s\beta^2} \frac{1}{u_2 - u_1} \Big[\log(u-u_2) - \log(u-u_1) \Big]_0^1 . \end{aligned} \tag{C.43}$$

This can then be written as

$$-\frac{4}{s\beta^2} \frac{1}{u_2 - u_1} \log \left| \frac{u_1 - u_1 u_2}{u_2 - u_1 u_2} \right| . \tag{C.44}$$

The variables u_1 and u_2 can be solved for using Eq. (C.41) and Eq. (C.40) such that

$$u_1 = \frac{1}{2}(1 - \sqrt{1 + \frac{4m^2}{s\beta^2}}) \,, \tag{C.45}$$

$$u_2 = \frac{1}{2}(1 + \sqrt{1 + \frac{4m^2}{s\beta^2}}) \,. \tag{C.46}$$

Using this we can rewrite Eq. (C.44) as

$$-\frac{4}{s\beta^2} \frac{1}{\sqrt{1 + \frac{m^2}{s\beta^2}}} \log \left| \frac{\frac{1}{2}(1 - \sqrt{1 + \frac{4m^2}{s\beta^2}}) + \frac{m^2}{s\beta^2}}{\frac{1}{2}(1 + \sqrt{1 + \frac{4m^2}{s\beta^2}}) + \frac{m^2}{s\beta^2}} \right| . \tag{C.47}$$

Rewriting this we get

$$-\frac{4}{s\beta^2} \frac{1}{\sqrt{1 + \frac{m^2}{s\beta^2}}} \log \left| \frac{\frac{1}{2}(1 - \sqrt{1 + \frac{4m^2}{s\beta^2}}) + \frac{m^2}{s\beta^2}}{\frac{1}{2}(1 + \sqrt{1 + \frac{4m^2}{s\beta^2}}) + \frac{m^2}{s\beta^2}} \right| = -\frac{8}{s\beta} \log \left| \frac{\beta - 1}{\beta + 1} \right| .$$

So using the definition $\gamma = \frac{1-\beta}{1+\beta}$ we can write

$$-\frac{8}{s\beta}\log|\gamma|\,. \tag{C.48}$$

So then the final partial integral takes the form

$$-\frac{8}{s\beta}\log|\gamma|\left(\log\frac{s_\gamma^{\max}-m_\pi^2}{m\cdot m_\pi}+\log\frac{m}{\Lambda}\right)-\int_0^1\frac{4}{VH}\operatorname{atanh}H\;\mathrm{d}u\,. \tag{C.49}$$

D List of δ_i and M_V^2 Terms

These δ and M_V^2 terms were determined from comparing the form factor model in one variable with the form of the ansatz.

VMD

The δ for the VMD is simply

$$\delta^{\mathrm{VMD}} = \{0,0,1\}\,. \tag{D.1}$$

The M_V^2 is in this case just the same as for the VMD model such that $M_{V,\mathrm{VMD}} = M_V$

LMD

For the LMD model the δ^{LMD} was found to be

$$\delta^{\mathrm{LMD}} = \left\{\frac{16F^4\pi^4}{(M_V^2N_C-4F^2\pi^2)^2}, -\frac{8(F^2M_V^2N_C\pi^2-8F^4\pi^4)}{(M_V^2N_C-4F^2\pi^2)^2}, \frac{(M_V^2N_C-8F^2\pi^2)^2}{(M_V^2N_C-4F^2\pi^2)^2}\right\}. \tag{D.2}$$

Similar to the VMD model the $M_{V,\mathrm{LMD}}$ is just $M_{V,\mathrm{LMD}} = M_V$.

TL

For the TL model the δ^{TL} is

$$\delta^{\mathrm{TL}} = \{1,4,4\}\,. \tag{D.3}$$

Similar to VMD and LMD have that $M_{V,\mathrm{TL}} = M_V$.

THS

For the THS model the situation is more complicated as two delta terms are necessary for computing the correction with two seperate M_V. First for convenience introduce

$$
\begin{aligned}
d_0 &= \frac{8F^4\pi^4}{(24F^2\pi^2 - N_C M_{V_2})^2}\,, \\
d_1 &= -(512F^4\pi^4(M_{V_2}^2 N_C - 8F^2(M_{V_1}^2 + 6M_{V_2}^2)\pi^2) + M_{V_1}^4 M_{V_2}^4\kappa) \\
&\quad \times \frac{(512F^4\pi^4(M_{V_1}^2 M_{V_2}^2 N_C + 4F^2(M_{V_1}^4 - 9M_{V_1}^2 M_{V_2}^2 - 6M_{V_2}^4)\pi^2) + M_{V_1}^4 M_{V_2}^6\kappa)}{131\,072F^8(M_{V_1} - M_{V_2})^3(M_{V_1} + M_{V_2})^3\pi^8(M_{V_2}^2 N_C - 24F^2\pi^2)^2}\,, \\
d_2 &= \frac{(512F^4\pi^4(M_{V_2}^4 N_C - 8F^2(M_{V_1}^2 + 6M_{V_2}^2)\pi^2) + M_{V_1}^4 M_{V_2}^4\kappa)^2}{262\,144F^8(M_{V_1}^2 - M_{V_2}^2)^2\pi^8(M_{V_2}^2 N_C - 24F^2\pi^2)^2} \\
D_0 &= d_0\,, \\
D_1 &= (512F^4\pi^4(M_{V_1}^2 M_{V_2}^2 N_C - 28F^2(M_{V_1}^2 + M_{V_2}^2)\pi^2) + M_{V_1}^4 M_{V_2}^4\kappa) \\
&\quad \times \frac{(512F^4\pi^4(M_{V_1}^2 M_{V_2}^4 N_C - 4F^2(M_{V_1}^4 + 14M_{V_1}^2 M_{V_2}^2 - M_{V_2}^4)\pi^2) + M_{V_1}^6 M_{V_2}^4\kappa)}{131\,072F^8(M_{V_1} - M_{V_2})^3(M_{V_1} + M_{V_2})^3\pi^8(M_{V_2}^2 N_C - 24F^2\pi^2)^2}\,, \\
D_2 &= \frac{(512F^4\pi^4(M_{V_1}^2 M_{V_2}^2 N_C - 28F^2(M_{V_1}^2 + M_{V_2}^2)\pi^2) + M_{V_1}^4 M_{V_2}^4\kappa)^2}{262\,144F^8(M_{V_1}^2 - M_{V_2}^2)^2\pi^8(M_{V_2}^2 N_C - 24F^2\pi^2)^2}\,.
\end{aligned}
$$

Then can write two δ terms

$$\delta^{\mathrm{THS}_1} = \{d_0, d_1, d_2\}\,, \tag{D.4}$$

$$\delta^{\mathrm{THS}_2} = \{D_0, D_1, D_2\}\,. \tag{D.5}$$

With $M_{V,\mathrm{THS}_1} = M_{V_1}$ and $M_{V,\mathrm{THS}_2} = M_{V_2}$, the full expression for the THS using the ansatz is then given by the sum of inserting the two δ terms.

References

[1] M. E. Peskin and D. V. Schroeder, *An Introduction to Quantum Field Theory*. Perseus Books, 1995.

[2] G. F. Sterman and P. Stoler, "Hadronic form-factors and perturbative QCD," *Ann. Rev. Nucl. Part. Sci.* **47** (1997) 193–233, arXiv:hep-ph/9708370.

[3] **Particle Data Group** Collaboration, P. Zyla *et al.*, "Review of Particle Physics," *PTEP* **2020** no. 8, (2020) 083C01.

[4] L. G. Landsberg, "Electromagnetic Leptonic Decays and Structure of Light Mesons," *Sov. Phys. Usp.* **28** (1985) 435–466.

[5] T. Husek, K. Kampf, S. Leupold, and J. Novotny, "Radiative corrections to the $\eta^{(\prime)}$ Dalitz decays," *Phys. Rev. D* **97** no. 9, (2018) 096013, arXiv:1711.11001 [hep-ph].

[6] T. Husek and S. Leupold, "Radiative corrections for the decay $\Sigma^0 \to \Lambda e^+ e^-$," *Eur. Phys. J. C* **80** no. 3, (2020) 218, arXiv:1911.02571 [hep-ph].

[7] T. Husek and S. Leupold, "Two-hadron saturation for the pseudoscalar–vector–vector correlator and phenomenological applications," *Eur. Phys. J. C* **75** no. 12, (2015) 586, arXiv:1507.00478 [hep-ph].

[8] M. D. Schartz, *Quantum Field Theory and the Standard Model*. Cambridge University Press, 2014.

[9] M. Gell-Mann and F. Zachariasen, "Form-factors and vector mesons," *Phys. Rev.* **124** (1961) 953–964.

[10] C. Terschlusen and S. Leupold, "Electromagnetic transition form factors of light vector mesons," *Phys. Lett. B* **691** (2010) 191–201, arXiv:1003.1030 [hep-ph].

[11] M. Knecht and A. Nyffeler, "Resonance estimates of O(p**6) low-energy constants and QCD short distance constraints," *Eur. Phys. J. C* **21** (2001) 659–678, arXiv:hep-ph/0106034.

[12] **NA60** Collaboration, R. Arnaldi *et al.*, "Study of the electromagnetic transition form-factors in $\eta \to \mu^+\mu^-\gamma$ and $\omega \to \mu^+\mu^-\pi^0$ decays with NA60," *Phys. Lett. B* **677** (2009) 260–266, arXiv:0902.2547 [hep-ph].

[13] R. I. Dzhelyadin *et al.*, "Study of the Electromagnetic Transition Form-factor in $\omega \to \pi^0\mu^+\mu^-$ Decay," *Phys. Lett. B* **102** (1981) 296.

[14] P. Adlarson *et al.*, "Measurement of the $\omega \to \pi^0 e^+ e^-$ and $\eta \to e^+e^-\gamma$ Dalitz decays with the A2 setup at MAMI," *Phys. Rev. C* **95** no. 3, (2017) 035208, arXiv:1609.04503 [hep-ex].

[15] **NA60** Collaboration, R. Arnaldi *et al.*, "Precision study of the $\eta \to \mu^+\mu^-\gamma$ and $\omega \to \mu^+\mu^-\pi^0$ electromagnetic transition form-factors and of the $\rho \to \mu^+\mu^-$ line shape in NA60," *Phys. Lett. B* **757** (2016) 437–444, arXiv:1608.07898 [hep-ex].